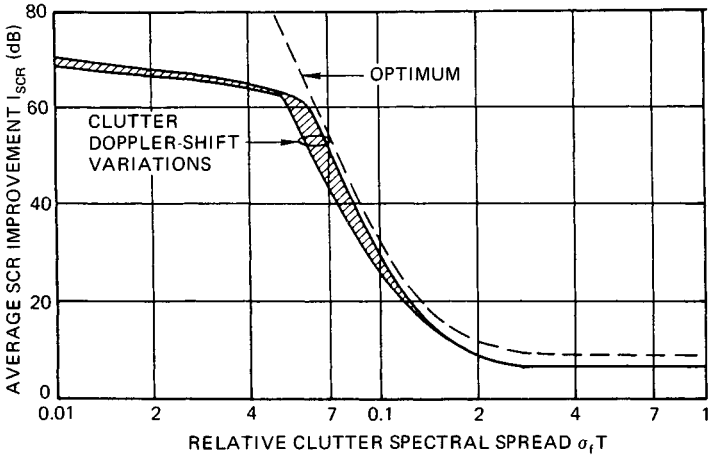

FIG. 15.30 Average SCR improvement for the 68 dB Chebyshev filter bank shown in Fig. 15.28. CPI = nine pulses. Optimum is from Fig. 15.19.

Fast Fourier Transform Filter Bank. For a large number of parallel doppler filters, hardware implementation can be significantly simplified through the use of the FFT algorithm. The use of this algorithm constrains all filters in the filter bank to have identical responses, and the filters will be uniformly spaced along the doppler axis. The number of filters implemented for a given size of the CPI can, however, be varied. For example, a larger number of filters can be realized by extending the received data with extra zero values (also known as zero padding) after the received returns have been appropriately weighted in accordance with the desired filter response (e.g., Chebyshev).

15.9 STAGGERED PRF

Stagger Design Procedures. The interval between radar pulses may be changed to shift the target velocities to which the MTI system is blind. The interval may be changed on a pulse-to-pulse, dwell-to-dwell (each dwell being a fraction of the beamwidth), or scan-to-scan basis. Each approach has advantages. The advantages of the scan-to-scan method are that the radar system is easier to build, and multiple-time-around clutter is canceled in a power amplifier MTI system. The transmitter stabilization necessary for good operation of an unstaggered MTI system costs money and weight. To stabilize the transmitter sufficiently for pulse-to-pulse or dwell-to-dwell stagger operation is considerably more difficult. Pulse-to-pulse staggering is used with MTI processing, while dwell-to-dwell staggering is used with filter bank processing.

For many MTI applications pulse-to-pulse staggering is essential. For example, if a binomial-weighted three-pulse canceler which has 36 percent–wide rejection notches is employed and if scan-to-scan pulse staggering is used, 36 percent of the desired targets would be missing on each scan owing to doppler considerations alone. This might be intolerable for some applications. With pulse-to-pulse staggering, good response can be obtained on all dopplers of interest on each scan. In addition, better velocity response can be obtained at some dopplers than

either pulse interval will give on a scan-to-scan basis. This is so because pulse-to-pulse staggering produces doppler components in the passband of the MTI filter. Pulse-to-pulse staggering may degrade the improvement factor attainable, as shown in Figs. 15.16 and 15.17, but this degradation may not be significant, or it can be eliminated by the use of time-varying weights as described below. One further advantage of pulse-to-pulse staggering is that it may permit eliminating the use of feedback in the cancelers (used to narrow the blind-speed notches), which simplifies canceler design.

The optimum choice of the stagger ratio depends on the velocity range over which there must be no blind speeds and on the permissible depth of the first null in the velocity response curve. For many applications, a four-period stagger ratio is best, and a good set of stagger ratios can be obtained by adding the first blind speed (in V/V_B) to the numbers -3, 2, -1, 3 (or 3, -2, 1, -3). Thus, in Fig. 15.31, where the first blind speed occurs at about $V/V_B = 28$, the stagger ratio is 25:30:27:31. (Alternating the long and short periods keeps the transmitter duty cycle as nearly constant as possible, as well as ensuring good response at the first null where $V = V_B$.) If using four interpulse periods permits the first null to be too deep, then five interpulse periods may be used, with the stagger ratio obtained by adding the first blind speed to the numbers -6, $+5$, -4, $+4$, $+1$. Figure 15.32 shows a velocity response curve for five pulse intervals. The depth of the first null can be predicted from Fig. 15.39, which is discussed later.

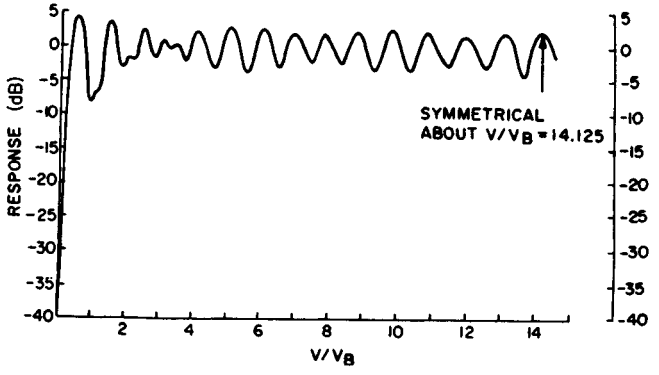

FIG. 15.31 Velocity response curve: dual canceler, no feedback, 25:30:27:31 pulse-interval ratio.

Figures 15.33 and 15.34 show two other velocity response curves calculated for four-pulse intervals. For a radar system with relatively few hits per beamwidth, it is not advantageous to use more than four or five different intervals because then the response to an individual target will depend on which part of the pulse sequence occurs as the peak of the beam passes the target. Random variation of the pulse intervals is not desirable (unless used as an electronic counter-countermeasure feature) because it permits the nulls to be deeper than the optimum choice of four- or five-pulse intervals.

When the ratio of pulse intervals is expressed as a set of relatively prime integers (i.e., a set of integers with no common divisor other than 1), the first true blind speed occurs at

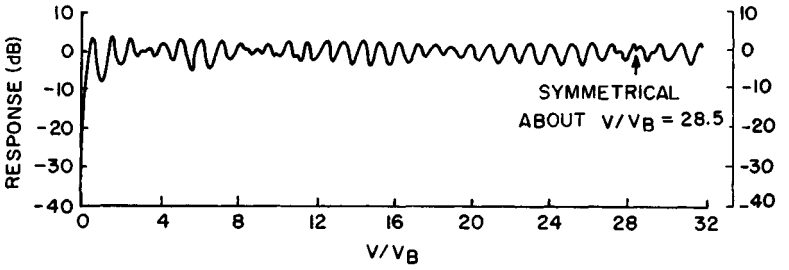

FIG. 15.32 Velocity response curve: three-pulse binomial canceler, 51:62:53:61:58 pulse-interval ratio.

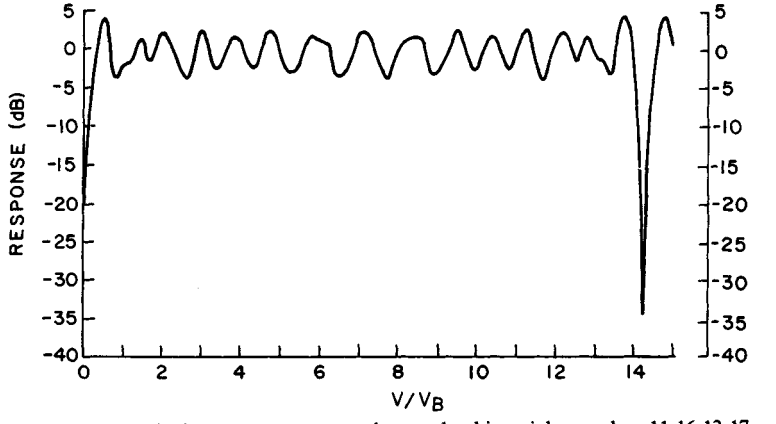

FIG. 15.33 Velocity response curve: three-pulse binomial canceler, 11:16:13:17 pulse-interval ratio.

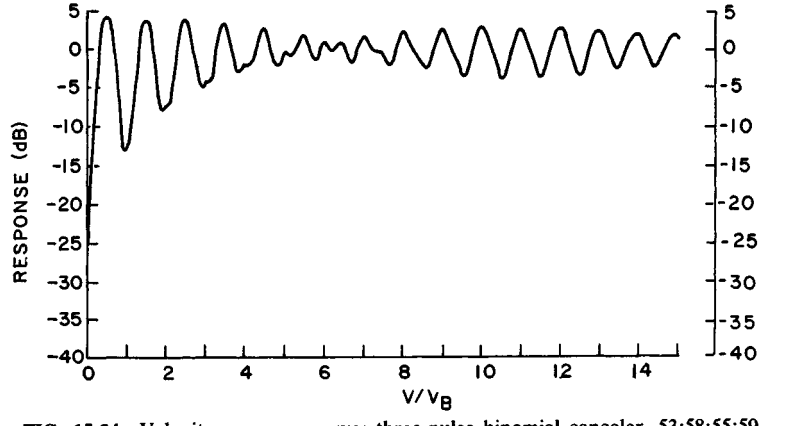

FIG. 15.34 Velocity response curve: three-pulse binomial canceler, 53:58:55:59 pulse-interval ratio. This response curve continues to $V/V_B = 53$ with no dips below 5 dB. The first blind speed is at $V/V_B = 56.25$.

$$\frac{V}{V_B} = \frac{R_1 + R_2 + R_3 + \cdots + R_N}{N} \tag{15.22}$$

where (R_1, R_2, R_3,..., R_N) are the set of integers and V_B is the blind speed corresponding to the average interpulse period. The velocity response curve is symmetrical about one-half of the value from Eq. (15.22). Thus, for the pulse-interval ratio 25:30:27:31, the first true blind speed occurs at $V/V_B = 28.25$, and the response curve is symmetrical about $V/V_B = 14.125$.

Feedback and Pulse-to-Pulse Staggering. When pulse-to-pulse staggering is employed, the effect of feedback is reduced. Staggering causes a modulation of the signal doppler at or near the maximum response frequency of the canceler. The amount of this modulation is proportional to the absolute target doppler so that, for an aircraft flying at V_B, the canceler response is essentially independent of the feedback employed. Figure 15.35 shows a plot of the effects of feedback on a dual-canceler system with 14.4 hits per beamwidth and a ratio of stagger intervals of 6:7:8. The feedback values employed are several of those used for the unstaggered velocity response plot in Fig. 15.22. If scan-to-scan pulse-interval staggering had been used instead of pulse-to-pulse, the no-feedback rms response for three scans at a target velocity of V_B would be −12.5 dB. The composite response for pulse-to-pulse staggering, however, is only −6 dB at V_B, thus illustrating the advantage of pulse-to-pulse staggering.

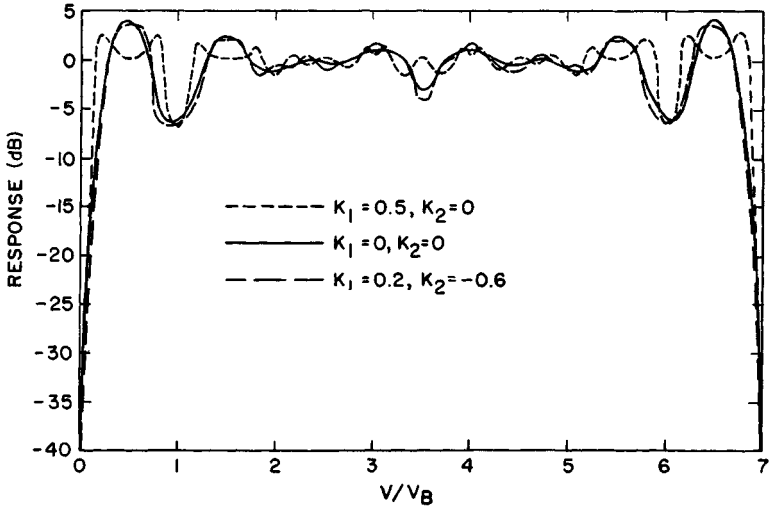

FIG. 15.35 Effect of feedback on the velocity response curve: dual canceler, 6:7:8 pulse-interval ratio.

Figure 15.36 shows the difference in response with a two-delay no-feedback canceler and with a three-delay canceler with a Chebyshev response (the same feedback used for the response in Fig. 15.23). These curves lie within about 3 dB of each other, except for velocities equal to $0.05V_B$ to $0.25V_B$. Since the radar signal from aircraft targets fluctuates considerably from scan to scan, for most

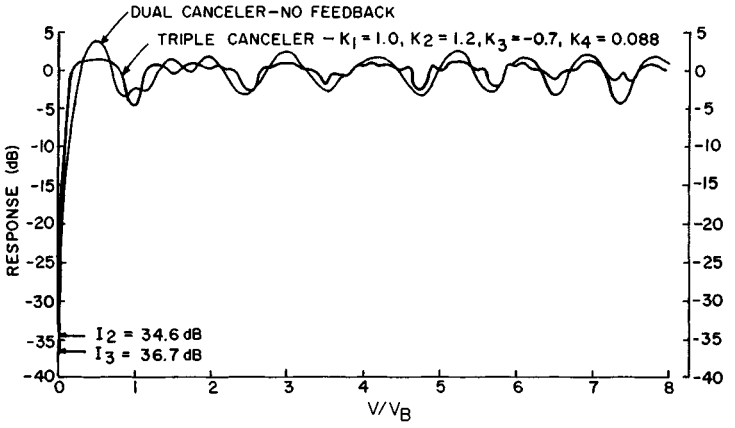

FIG. 15.36 Velocity response curves: triple canceler with no feedback; 12:16:13:18 pulse-interval ratio.

surveillance radar applications there is no practical advantage in employing the more complex canceler.

Figure 15.37 shows the difference in response between a five-pulse feedforward canceler and a three-pulse feedback canceler (the same such cancelers depicted in Fig. 15.25) for stagger ratios of 17:19:21:23. Although the feedback canceler response ripples more than the five-pulse feedforward canceler, no significant system advantage would accrue for the five-pulse canceler unless it is used in a batch mode, or step-scan mode, where the finite transient-response time

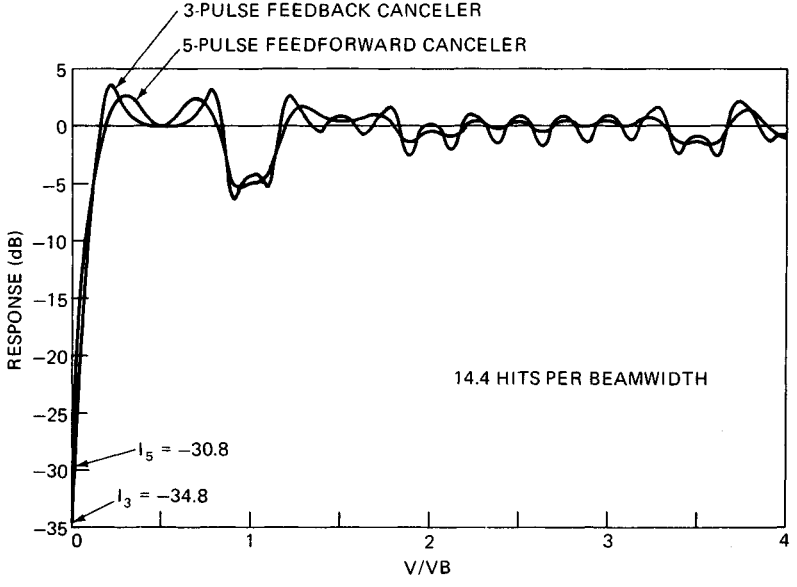

FIG. 15.37 Velocity response curves: five-pulse feedforward canceler and three-pulse feedback canceler of Fig. 15.25 for a 17:19:21:23 pulse-interval ratio.

becomes important (as discussed above, in Fig. 15.25 the four-pulse filter would be preferable to the five-pulse filter).

In some staggered systems, the use of feedback may serve a useful purpose: to increase the improvement factor of the system. Whether the feedback will help significantly depends on whether the stagger ratio or the scanning modulation limits the system performance more severely. If the limitation is primarily from scanning modulation, the feedback may be of some help.

Improvement Factor Limitations Caused by Staggering. When pulse-to-pulse staggering is used, it limits the attainable improvement factor owing to the unequal time spacing of the received clutter samples. The curves in Figs. 15.16 and 15.17, which have been referred to several times, give the approximate limitation on I caused by pulse-to-pulse staggering and either antenna scanning or internal clutter motion. They have been derived as explained below.

A two-delay canceler will perfectly cancel a linear waveform, $V(t) = c + at$, if it is sampled at equal time intervals independent of the constant c or the slope a. [Additional delay cancelers perfectly cancel additional waveform derivatives; e.g., a three-delay canceler will perfectly cancel $V(t) = c + at + bt^2$.] A stagger system with two pulse intervals samples the linear waveform at unequal intervals, and therefore there will be a voltage residue from the cancelers that is proportional to the slope a and inversely proportional to $\gamma - 1$, where γ is the ratio of the intervals. The apparent doppler frequency of the residue will be at one-half the average repetition rate of the system and thus will be at the frequency of maximum response of a no-feedback canceler.

The rate of change of phase or amplitude of clutter signals in a scanning radar is inversely proportional to the hits per beamwidth, n. Thus, with the use of a computer simulation to determine the proportionality constant, the limitation on I due to staggering is approximately

$$I \approx 20 \log \left(\frac{2.5n}{\gamma - 1} \right) \quad \text{dB} \tag{15.23}$$

which is plotted in Fig. 15.16.

These curves, which apply to all multiple-delay cancelers, give answers that are fairly close to the actual limitation that will be experienced for most practical stagger ratios. An example of the accuracy is as follows: A system with 14.4 hits per beamwidth, a four-pulse binomial weight canceler, and a 6:9:7:8 pulse-interval ratio has an improvement factor limitation of 36.5 dB due to staggering. The curve gives a limitation of 37.2 dB for this case. But note that if the sequence of pulse intervals is changed from 6:9:7:8 to 6:8:9:7, the actual limitation is 41.1 dB, which is 3.9 dB less than that indicated by the curve. This occurs because the primary modulation with a 6:9:7:8 pulse-interval ratio looks like a target at maximum-response speed, whereas the primary modulation with a 6:8:9:7 pulse-interval ratio looks like a target at one-half the speed of maximum response. Because it is desirable to average the transmitter duty cycle over as short a period as possible, the 6:9:7:8 pulse-interval ratio would probably be chosen for a practical system.

Once Eq. (15.23) for the limitation on I due to scanning and staggering is obtained, it is possible to determine the limitation on I due to internal-clutter motion and staggering. If

$$n = \frac{\sqrt{1n(2)}}{2\pi} \times \frac{\lambda f_r}{\sigma_v} = 0.1325 \frac{\lambda f_r}{\sigma_v} \tag{15.24}$$

[from Eqs. (15.4) and (15.5)] is substituted into Eq. (15.23),

$$I = 20 \log \left(\frac{2.5}{\gamma - 1} \times \frac{0.1325\lambda f_r}{\sigma_v} \right) = 20 \log \left(\frac{0.33\lambda f_r}{(\gamma - 1)\sigma_v} \right) \tag{15.25}$$

where λ is the wavelength, f_r is the average pulse repetition frequency, and σ_v is the rms velocity spread of scattering elements. This is plotted in Fig. 15.17 for rain and for wooded hills with a 40-kn wind. This limitation on the MTI improvement factor is independent of the type of canceler employed.

Time-Varying Weights. The improvement factor limitation caused by pulse-to-pulse staggering can be avoided by the use of time-varying weights in the canceler forward paths instead of binomial weights. The use of time-varying weights has no appreciable effect on the MTI velocity response curve. Whether the added complexity of utilizing time-varying weights is desirable depends on whether the stagger limitation is predominant. For two-delay cancelers, the stagger limitation is often comparable with the basic canceler capability without staggering. For three-delay cancelers, the stagger limitation usually predominates.

Consider the transmitter pulse train and the canceler configurations shown in Fig. 15.38. During the interval T_N when the returns from transmitted pulse P_N are being received, the two-delay canceler weights should be

$$A = 1 \qquad C = \frac{T_{N-2}}{T_{N-1}} \qquad B = -1 - C \tag{15.26}$$

and the three-delay canceler weights should be

$$A = 1 \qquad C = 1 + \frac{T_{N-3} + T_{N-1}}{T_{N-2}}$$

$$B = -C \qquad D = -1 \tag{15.27}$$

These weights have been derived by assuming that the cancelers should perfectly cancel a linear waveform $V(t) = c + at$, sampled at the stagger rate, independently of the values of the constant c or the slope a. [As mentioned at the beginning of this section, a multiple-delay canceler with binomial weights in an unstaggered system will perfectly cancel $V(t) = c + at$.]

The choice of $A = 1$ in both cases is arbitrary. In the three-delay canceler, setting $D = -1$ eliminates the opportunity for a second-order correction to cancel the quadratic term bt^2 which could be obtained if D were also time-varying. Computer calculations have shown that it is unnecessary to vary D in most practical systems.

Depth of First Null in Velocity Response. When selecting system parameters, it is useful to know the depth of the first few nulls to be expected in the velocity response curve. As discussed earlier, the null depths are essentially unaffected by feedback. They are also essentially independent of the type of canceler employed, whether single, dual, or triple, or of the number of hits per beamwidth. Figure 15.39 shows approximately what null depths can be expected versus the ratio of maximum to minimum interpulse period.

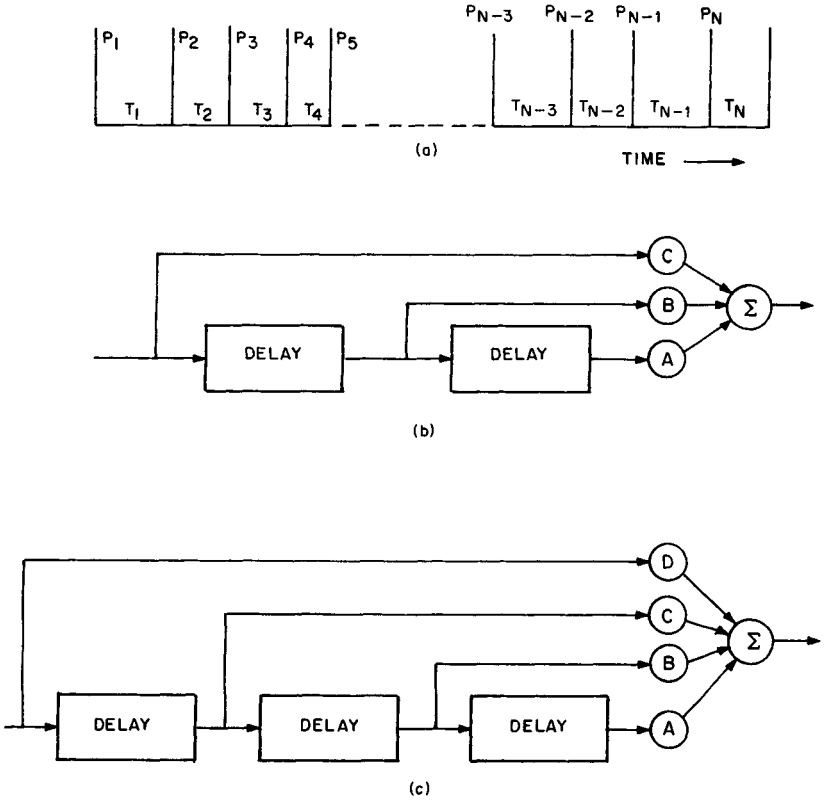

FIG. 15.38 Use of time-varying weights. (*a*) Pulse train. (*b*) Two-delay canceler. (*c*) Three-delay canceler.

15.10 IMPROVEMENT FACTOR RESTRICTION CAUSED BY LIMITING

Field measurements have indicated that the performance of many scanning multiple-delay MTI radar systems falls considerably short of the performance predicted above. This is true because the above theory is based on the assumption that the system is linear. As described earlier, many MTI systems use a linear-limiting amplifier preceding the canceler to adjust clutter residue to the level of thermal noise. Sometimes inadvertent clutter signal limiting occurs because of insufficient receiver dynamic range.

An example of how limiting the dynamic range adjusts the residue is shown in the MTI PPI photographs of Fig. 15.40. The range rings are at 5-mi intervals. A number of birds are shown on the display. The residue from clutter in the left photograph is solid out to 3 nmi and then decreases until it is almost entirely gone at 10 nmi. The MTI improvement factor in both pictures is 18 dB, but the input dynamic range (peak signal-to-rms noise) to the canceler was changed from 20 to 14 dB between the two pictures. An aircraft flying over the clutter in the first 5 mi in the left-hand picture could not be detected, no matter how large its radar cross

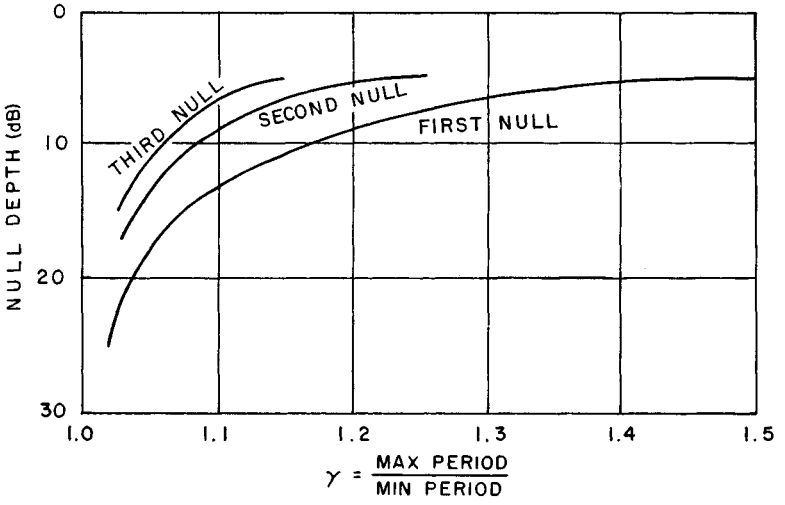

FIG. 15.39 Approximate depth of nulls in the velocity response curve for pulse-to-pulse staggered MTI.

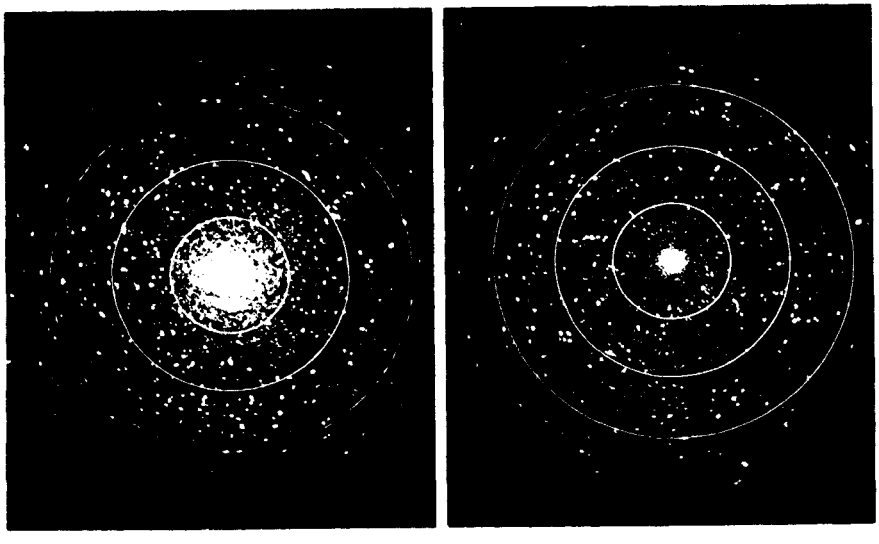

(*a*) (*b*)

FIG. 15.40 Effect of limiters. (*a*) 18 dB improvement factor, 20 dB input dynamic range. (*b*) 18 dB improvement factor, 14 dB input dynamic range.

section. In the right-hand picture, the aircraft could be detected if the target-to-clutter cross-section ratio were sufficient.

Prior to the development of modern clutter maps for controlling false alarms caused by clutter residue, the use of IF limiting was essential for false-alarm control in an MTI radar. Such limiting, however, seriously affects the improvement

obtainable with a scanning-limited, multiple-delay canceler because of the increased spectral spread of the clutter that exceeds the limit level. Part of the additional clutter spectral components comes from the sharp discontinuity in the envelope of returns as the clutter reaches the limit level.[24] A time-domain example of this phenomenon is shown in Fig. 15.41 for a radar with 16.4 hits per beamwidth. On the left is a point target that does not exceed the limit level; on the right is a point target that exceeds the limit level by 20 dB. Note that, for this example, I degrades by 12.8 dB for the dual canceler and by 26.5 dB for the triple canceler. The exact result of this calculation depends on the assumed shape of the antenna pattern. [In this case, a (sin U)/U pattern terminated at the first nulls was assumed.] There is a comparable spectral spread of limited distributed

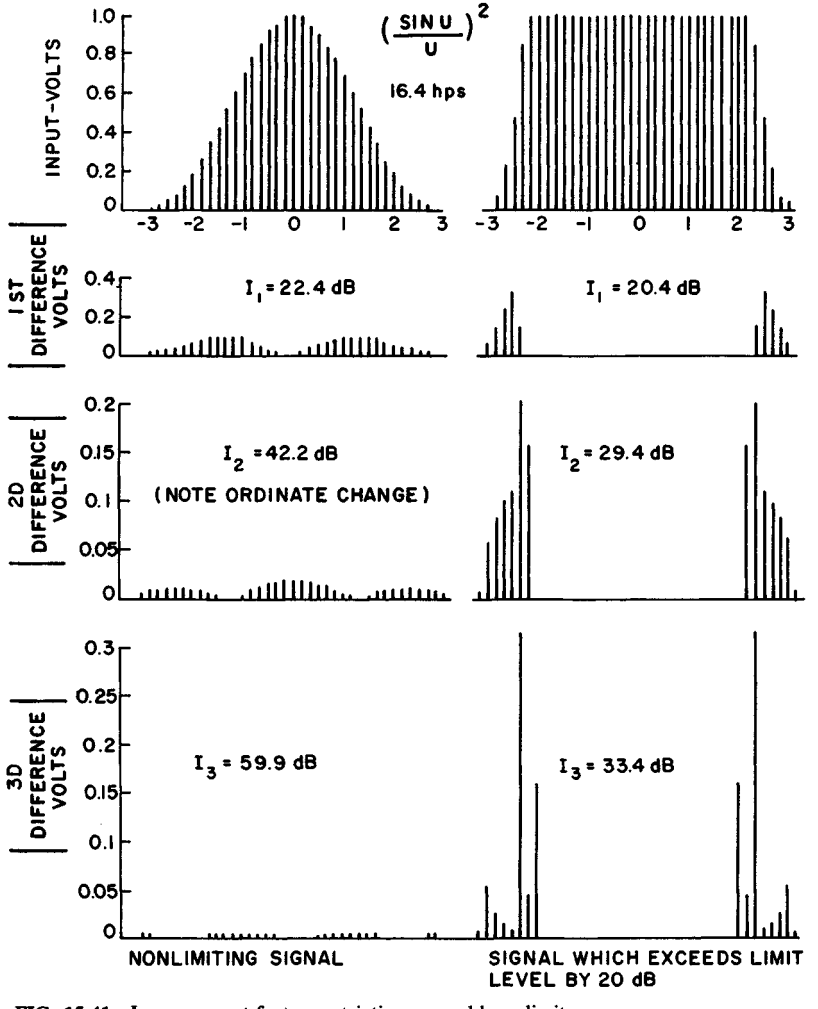

FIG. 15.41 Improvement factor restriction caused by a limiter.

clutter.[25,26] Figure 15.42*a*, *b*, and *c*, from Ref. 25, shows the expected improvement factor for two- three-, and four-pulse cancelers as a function of σ/L, the ratio of the rms clutter amplitude to the limit level. Hits per one-way half-power beamwidth are indicated by n.

When limiting is used for controlling false alarms, the dynamic range must be adjusted so that the residue from clutter is approximately equal to receiver noise. If this is not done, the clutter residue will be so strong that it will be impossible to detect desired targets in the clutter area. (It is possible to track a target through a clutter area with considerably more residue than permits initial detection of a target, but for surveillance and detection purposes the operators must have a clean display.)

Because MTI systems are built so that the dynamic range of signals into the canceler can be adjusted in the field to provide a good display, actual performance often falls far short of assumed performance without the user being aware of the difference.

With the proper employment of clutter maps, as described in Sec. 15.14, MTI radars can be operated with much larger dynamic ranges, and the degradation caused by IF limiters can be greatly reduced or eliminated.

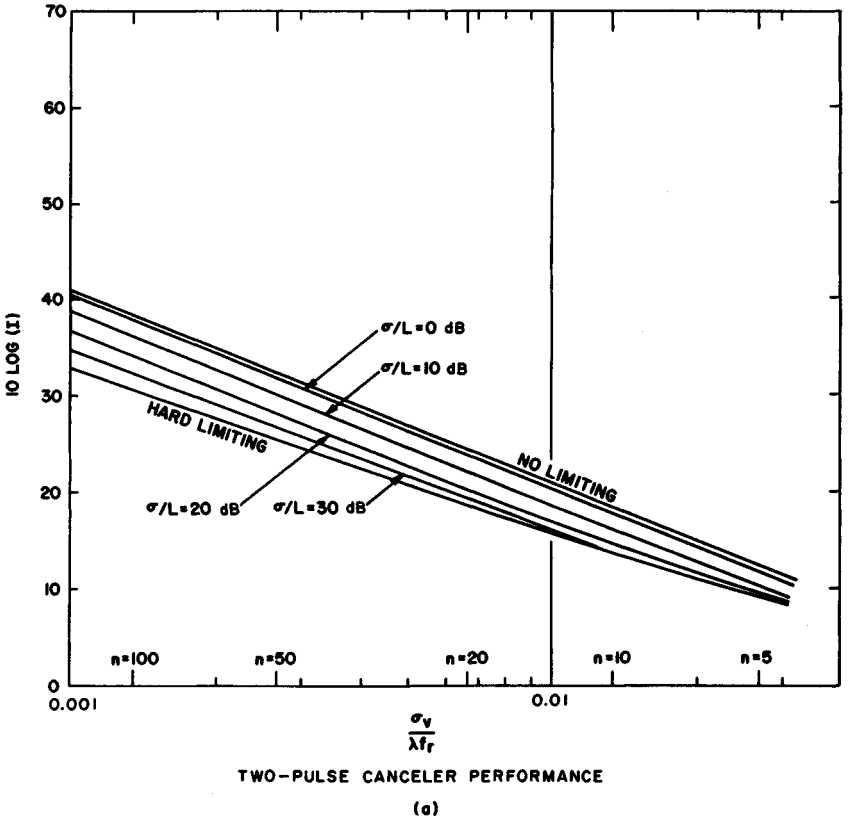

FIG. 15.42 Improvement factor restriction versus amount of limiting and clutter spectral spread. (*a*) Two-pulse canceler. (*b*) Three-pulse canceler. (*c*) Four-pulse canceler.

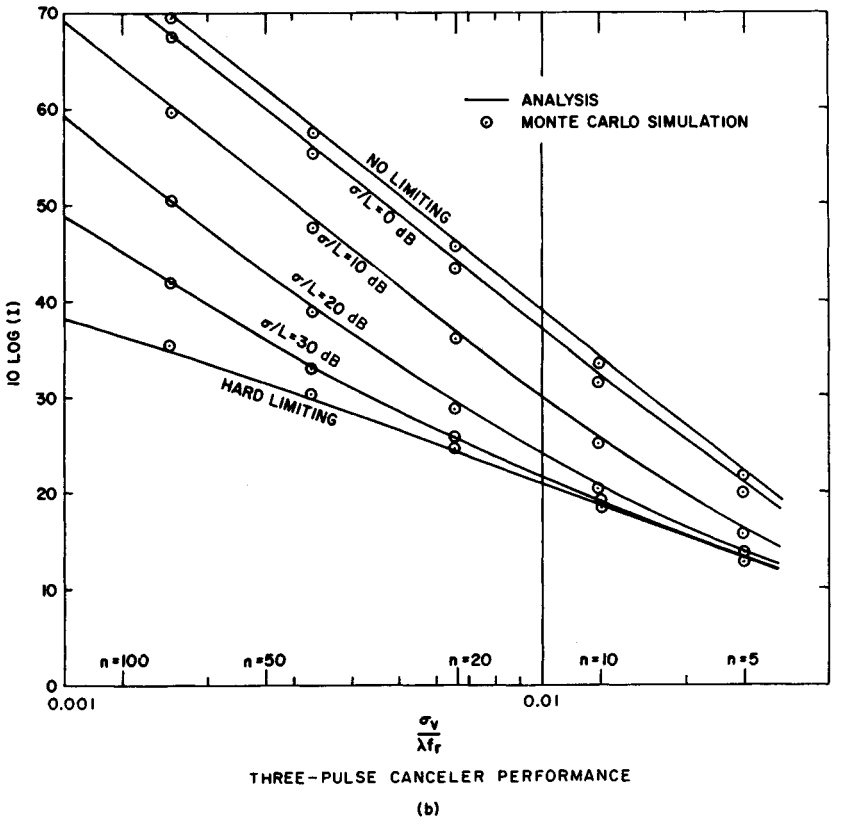

FIG. 15.42 *(Continued)*

15.11 RADAR SYSTEM STABILITY AND A/D QUANTIZATION REQUIREMENTS

System Instabilities. Not only do clutter motion and scanning affect the MTI improvement factor attainable, but system instabilities also place a limit on MTI performance. These instabilities come from the stalo and coho, from the transmitter pulse-to-pulse frequency change if a pulsed oscillator and from pulse-to-pulse phase change if a power amplifier, from the inability to lock the coho perfectly to the phase of the reference pulse, from time jitter and amplitude jitter on the pulses, and from quantization noise of the A/D converter. Weil has presented an excellent detailed discussion of these effects.[27,28]

Phase instabilities will be considered first. If the phases of consecutive received pulses relative to the phase of the coho differ by, say, 0.01 rad, a limitation of 40 dB is placed on the improvement factor possible. The 0.01-rad clutter vector change is equivalent to a target vector 40 dB weaker than the clutter su-

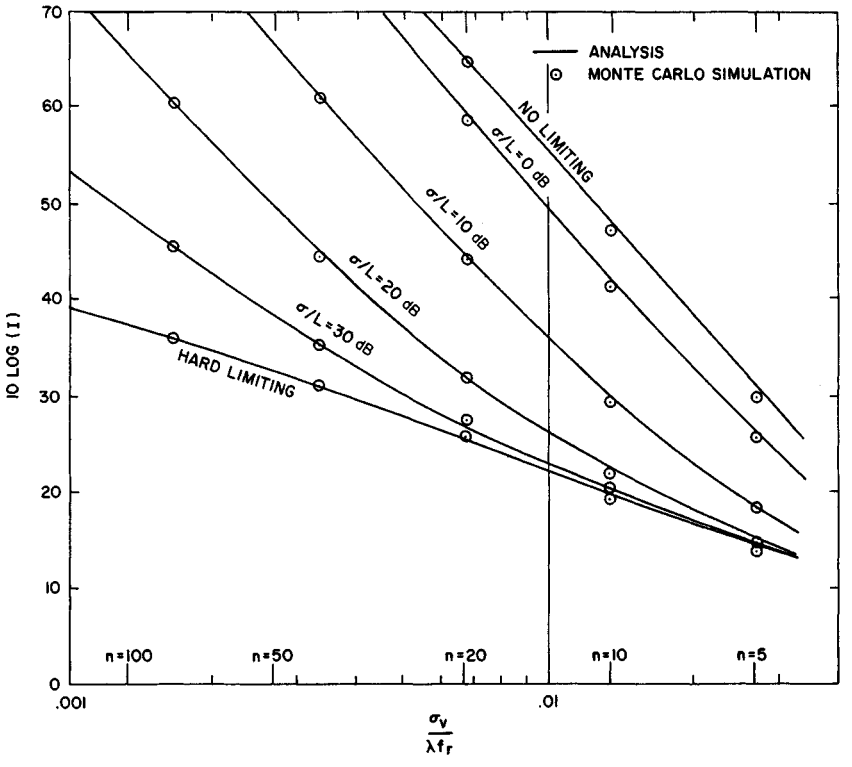

FIG. 15.42 *(Continued)*

perimposed on the clutter, as shown in Fig. 15.43.

In the power amplifier MTI system shown in Fig. 15.44, pulse-to-pulse phase changes in the transmitted pulse can be introduced by the pulsed amplifier. The most common cause of a power amplifier introducing phase changes is ripple on

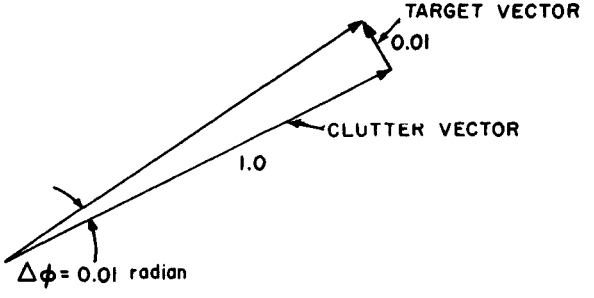

FIG. 15.43 Phase instability.

the high-voltage power supply. Other causes of phase instability include ac voltage on the transmitter tube filament and uneven power supply loading, such as that caused by pulse-to-pulse stagger.

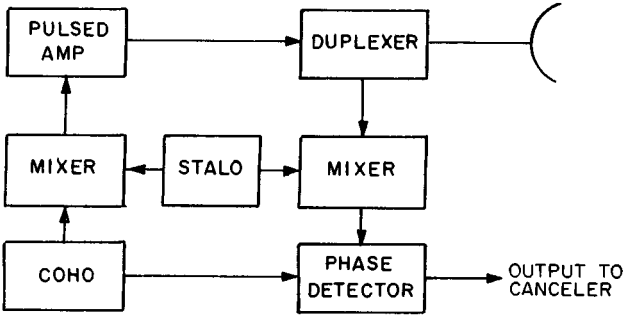

FIG. 15.44 Power amplifier simplified block diagram.

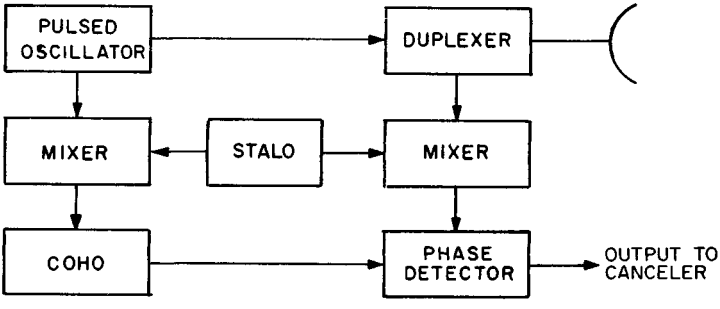

FIG. 15.45 Pulsed oscillator simplified block diagram.

In the pulsed oscillator system, shown in Fig. 15.45, pulse-to-pulse frequency changes result in phase run-out during the transmitted pulse. Phase run-out is the change of the transmitted pulse during the pulse duration with respect to the phase of the reference oscillator. If the coho locked perfectly to the end of the transmitted pulse, a total phase run-out of 0.02 rad during the transmitted pulse would then place an average limitation of 40 dB on the improvement factor attainable. Pulse-to-pulse frequency change in microwave oscillators is primarily caused by high-voltage power supply ripple. In the pulsed oscillator system, a pulse-to-pulse phase difference of 0.01 rad in locking the coho results in an improvement factor limitation of 40 dB.

The limitations on the improvement factor which are due to equipment instabilities in the form of frequency changes of the stalo and coho between consecutive transmitted pulses are a function of the range of the clutter. These changes are characterized in two ways. All oscillators have a noise spectrum. In addition, cavity oscillators, used because they are readily tunable, are microphonic, and thus their frequency may vary at an audio rate. The limitation on the improvement factor due to frequency changes is the difference in the number of radians

that the oscillator runs through between the time of transmission and the time of reception of consecutive pulses. Thus the improvement factor will be limited to 40 dB if $2\pi\Delta fT = 0.01$ rad, where Δf is the oscillator frequency change between transmitted pulses and T is the transit time of the pulse to and from the target.

To evaluate the effects of oscillator phase noise on MTI performance, there are four steps. First, determine the single-sideband power spectral density of the phase noise as a function of frequency from the carrier.[29,30] Second, increase this spectral density by 6 dB. This accounts for a 3 dB increase because both sidebands of noise affect clutter residue and a 3 dB increase because the oscillator contributes noise during both transmitting and receiving. Third, adjust the spectral density for (*a*) correlation due to the range of the clutter of interest, (*b*) noise rejection due to the frequency response of the clutter filters, and (*c*) the frequency response of the receiver passband. Fourth, integrate the adjusted spectral density of the phase noise. The result is the limitation on the improvement factor due to the oscillator noise. Oscillator phase noise and adjustments to phase noise can all be approximated by straight lines on a decibel-versus-log frequency plot. The places where the straight lines intersect are called break frequencies.

The first adjustment, correlation due to range of the clutter of interest, reduces noise at the low frequencies by 20 dB per decade from the break frequency at $f = c/(2\pi R)$, where c is the speed of light and R is the clutter range. For the second adjustment, the response at low frequency of the clutter filters, cancelers with binomial weights have responses that fall off at 20 dB per decade for one delay, 40 dB per decade for two delays, 60 dB per decade for three delays, etc. The break frequencies for the start of the response falloff are $0.225f_r$ for one delay, $0.249f_r$ for two delays, $0.262f_r$ for three delays, and $0.271f_r$ for four delays. (If the clutter filters do not use binomial weights, the exact filter response must be used.) At frequencies higher than the start of the filter passband, the clutter filter is assumed to have unity gain because the average noise gain is unity.

For example, consider an oscillator (*oscillator* is assumed to include the complete microwave signal source, which typically includes a crystal oscillator and a multiplier chain) with single-sideband phase-noise spectral density as shown in Fig. 15.46. (One device for measuring phase noise is the Hewlett Packard 11729B Carrier Noise Test Set.[30]) The single-sideband noise is increased by 3 dB because both sidebands affect system stability and by an additional 3 dB because the oscillator introduces noise in both the transmitted signal (or coho locking signal if a magnetron transmitter is used) and the receiver downconversion process. Figure 15.47 shows the spectral modifications due to the system response. (*a*) The first modification accounts for correlation due to the range to the clutter of interest [assumed clutter range is $\approx$ 100 nmi (185.2 km); thus the break frequency is $3 \times 10^8/(2\pi \times 185{,}200) = 365$ Hz]. (*b*) Second, a three-pulse binomial-weighted canceler is assumed with the radar operating at a PRF of 360 Hz. Thus the break frequency is $0.249 \times 360 = 90$ Hz. (*c*) Third, the receiver passband is assumed to extend from -500 kHz to $+500$ kHz with respect to the IF center frequency (1-MHz total passband) at the -3 dB points and determined by a two-pole filter. Thus the receiver passband response falls off at 40 dB per decade from the break frequency at 500 kHz as shown.

The modified phase-noise spectral density is shown in Fig. 15.48. The total noise power with respect to the carrier is determined by integration of the noise power under the curve. The equation for spectral power density of each segment as a function of frequency is

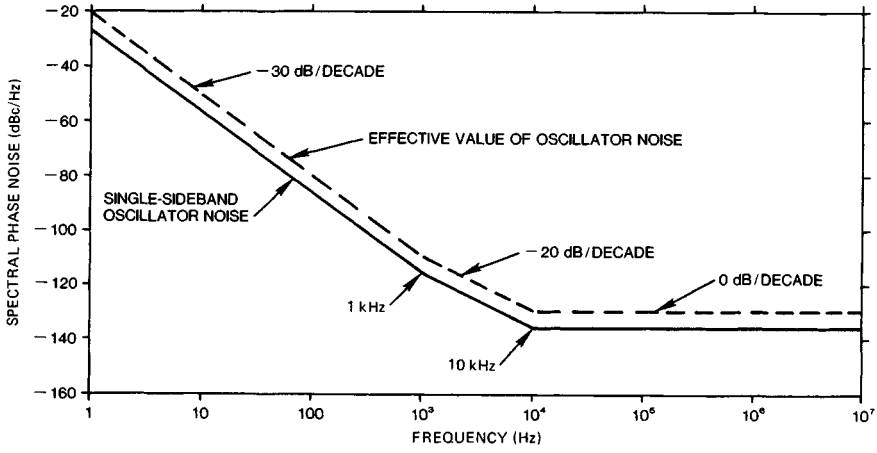

FIG. 15.46 Single-sideband phase-noise spectral density of a microwave oscillator and the effective noise density.

$$P(f) = P_{f1} \times 10^{\left[\frac{\text{SLOPE}}{10} \log\left(\frac{f}{f_1}\right)\right]} \tag{15.28}$$

where P_{f1} is spectral power density, in watts per hertz, at f_1 (for convenience, it is assumed that the carrier power is 1 W); SLOPE is the slope of the segment, in decibels per decade; and f_1 is the frequency where P_{f1} is specified.

For each segment of the spectrum with constant slope, this equation can be integrated by using Vigneri's method[31] or with calculators with an integrate function, such as the Hewlett Packard HP-15C. Table 15.3 gives the integration for the example. Note that the assumption is made that the carrier power is 1 W, so that, for example, −149.4 dBc/Hz becomes 1.148×10^{-15} W/Hz. When the integrated powers for all the segments are calculated, they are summed and then

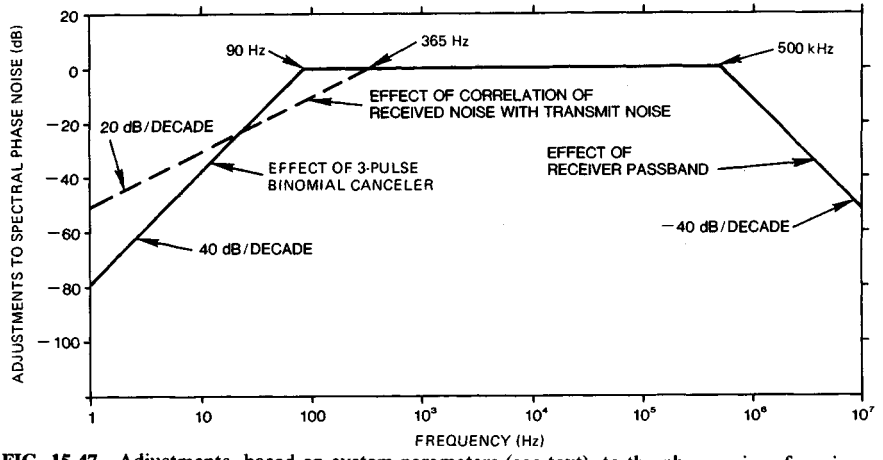

FIG. 15.47 Adjustments, based on system parameters (see text), to the phase noise of a microwave oscillator.

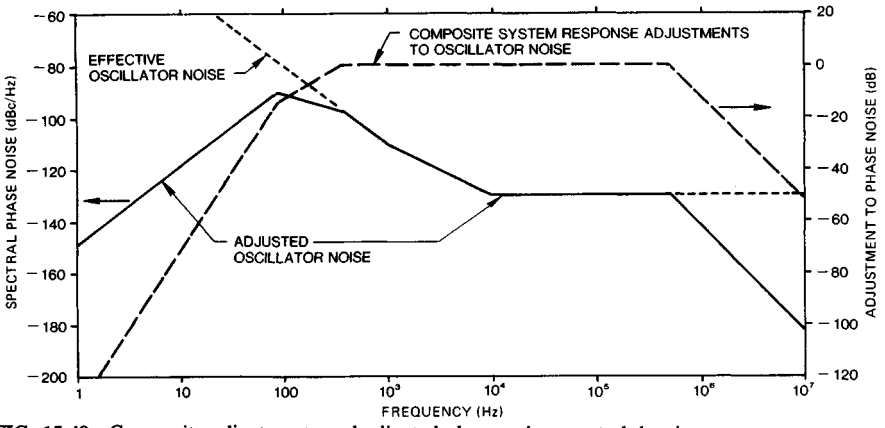

FIG. 15.48 Composite adjustments and adjusted phase-noise spectral density.

TABLE 15.3 Integration of the Phase-Noise Spectral Density of Fig. 15.46 with Adjustments of Fig. 15.47 as Shown in Fig. 15.48

Segment	f_1, Hz	f_2, Hz	Slope, decibels per decade	P_1, dBc/Hz	Integrated power, W	Integrated power, dBc
1	1	90	30.0	−149.4	0.188E-07	−77.25
2	90	365	−10.0	−90.8	0.105E-06	−69.80
3	365	1,000	−30.0	−96.9	0.323E-07	−74.91
4	1,000	10,000	−20.0	−110.0	0.900E-08	−80.46
5	10,000	500,000	0.0	−130.0	0.490E-07	−73.10
6	500,000	1,000,000	−40.0	−130.0	0.167E-07	−77.78
	Total integrated noise power				0.231E-06	− 66.37

converted back to dBc. The final answer, −66.37 dBc, is the limit on I that results from oscillator noise. The limit on I_{SCR} (dB) is I (dB) plus target integration gain (dB).

Time jitter of the transmitted pulses results in degradation of MTI systems. Time jitter results in failure of the leading and trailing edges of the pulses to cancel, the amplitude of each uncanceled part being $\Delta t/\tau$, where Δt is the time jitter and τ is the transmitted pulse length. The total residue power is $2(\Delta t/\tau)^2$, and therefore the limitation on the improvement factor due to time jitter is $I = 20 \log [\tau/(\sqrt{2}\,\Delta t)]$ (dB). This limit on the improvement factor is based on an uncoded transmitter pulse and on the assumption that the receiver bandwidth is matched to the duration of the transmitted pulse. In a pulse compression system, the receiver bandwidth is wider by the time-bandwidth ($B\tau$) product; thus the clutter residue power at each end of the pulse increases in proportion to the $B\tau$ product. The limit on I for a chirp pulse compression system is then $I = 20 \log [\tau/(\sqrt{2}\,\Delta t\,\sqrt{B\tau})]$. For pulse compression systems employing burst waveforms, the factor 2 in the preceding equation should be multiplied by the number of subpulses in the waveform. Thus, for example, the limit on I for a 13-pulse Barker code is

$$I = 20 \log [\tau/(\sqrt{2 \times 13}\ \Delta t \sqrt{13})] \quad \text{dB} \tag{15.29}$$

Pulse-width jitter results in one-half the residue of time jitter, and

$$I = 20 \log \frac{\tau}{\Delta \text{PW} \sqrt{B\tau}} \quad \text{dB} \tag{15.30}$$

where ΔPW is pulse-width jitter.

Amplitude jitter in the transmitted pulse also causes a limitation of

$$I = 20 \log \frac{A}{\Delta A} \quad \text{dB} \tag{15.31}$$

where A is the pulse amplitude and ΔA is the pulse-to-pulse change in amplitude. This limitation applies even though the system uses limiting before the canceler because there is always present much clutter that does not reach the limit level. With most transmitters, however, the amplitude jitter is insignificant after the frequency-stability or phase-stability requirements have been met.

Jitter in the sampling time in the A/D converter also limits MTI performance. If pulse compression is done prior to the A/D or if there is no pulse compression, this limit is

$$I = 20 \log \frac{\tau}{J \sqrt{B\tau}} \quad \text{dB} \tag{15.32}$$

where J is the timing jitter, τ is transmitted pulse length, and $B\tau$ is the time-bandwidth product. If pulse compression is done subsequent to the A/D converter, then the limitation is

$$I = 20 \log \frac{\tau}{JB\tau} \quad \text{dB} \tag{15.33}$$

The limitations on the attainable MTI improvement factor are summarized in Table 15.4. This discussion has assumed that the peak-to-peak values of these instabilities occur on a pulse-to-pulse basis, which is often the case in pulse-to-pulse staggered MTI operation. If it is known that the instabilities are random, the peak values shown in these equations can be replaced by the rms pulse-to-pulse values, which gives results essentially identical to Steinberg's results.[32]

If the instabilities occur at some known frequency, e.g., high-voltage power supply ripple, the relative effect of the instability can be determined by locating the response on the velocity response curve for the MTI system for a target at an equivalent doppler frequency. If, for instance, the response is 6 dB down from the maximum response, the limitation on I is about 6 dB less severe than indicated in the equations in Table 15.4.

If all sources of instability are independent, as would usually be the case, their individual power residues can be added to determine the total limitation on MTI performance.

Intrapulse frequency or phase variations do not interfere with good MTI operation provided they repeat precisely from pulse to pulse. The only concern is a

TABLE 15.4 Instability Limitations

Pulse-to-pulse instability	Limit on improvement factor
Transmitter frequency	$I = 20 \log [1/(\pi\, \Delta f\, \tau)]$
Stalo or coho frequency	$I = 20 \log [1/(2\pi\, \Delta f\, T)]$
Transmitter phase shift	$I = 20 \log (1/\Delta\phi)$
Coho locking	$I = 20 \log (1/\Delta\phi)$
Pulse timing	$I = 20 \log [\tau/(\sqrt{2}\Delta t \sqrt{B\tau})]$
Pulse width	$I = 20\log[\tau/(\Delta PW \sqrt{B\tau})]$
Pulse amplitude	$I = 20 \log (A/\Delta A)$
A/D jitter	$I = 20 \log [\tau(J \sqrt{B\tau})]$
A/D jitter with pulse compression following A/D	$I = 20 \log [\tau/(JB\tau)]$

where Δf = interpulse frequency change
τ = transmitted pulse length
T = transmission time to and from target
$\Delta\phi$ = interpulse phase change
Δt = time jitter
J = A/D sampling time jitter
$B\tau$ = time-bandwidth product of pulse compression system ($B\tau$ = unity for uncoded pulses)
ΔPW = pulse-width jitter
A = pulse amplitude, V
ΔA = interpulse amplitude change

loss of sensitivity if phase run-out during the transmitted pulse or mistuning of the coho or stalo permits the received pulses to be significantly detuned from the intended IF frequency. If 1-rad phase run-out during the pulse is permitted, the system detuning may be as large as $1/(2\pi\tau)$ Hz with no degradation of MTI performance.

To give an example of interpulse-stability requirements, consider a 3000-MHz radar transmitting an uncoded 2-μs pulse and the requirement that no single system instability will limit the MTI improvement factor attainable at a range of 100 nmi to less than 50 dB, a voltage ratio of 316:1.

The rms pulse-to-pulse transmitter frequency change (if a pulsed oscillator) must be less than

$$\Delta f = \frac{1}{316\pi\tau} = 504 \text{ Hz}$$

which is a stability of about 2 parts in 10^7.

The rms pulse-to-pulse transmitter phase-shift change (if a power amplifier) must be less than

$$\Delta\phi = \frac{1}{316} = 0.00316 \text{ rad} = 0.18°$$

The stalo or coho frequency change must be less than

$$\Delta f = \frac{1}{316\ (2\pi)\ (100 \times 12.36 \times 10^{-6})} = 0.4 \text{ Hz}$$

which is a short-term stability of 1 part in 10^{10} for the stalo (at about 3 GHz) and 1 part in 10^8 for the coho (assuming a 30-MHz IF frequency).

The coho locking (if a pulsed oscillator system) must be within

$$\Delta\phi = \frac{1}{316} = 0.00316 \text{ rad} = 0.18°$$

The pulse timing jitter must be less than

$$\Delta t = \frac{\tau}{316\sqrt{2}\sqrt{1}} = \frac{2 \times 10^{-6}}{316\sqrt{2}} = 4.5 \times 10^{-9} \text{ s}$$

The pulse-width jitter must be less than

$$\Delta\text{PW} = \frac{\tau}{316\sqrt{1}} = \frac{2 \times 10^{-6}}{316} = 6 \times 10^{-9} \text{ s}$$

The pulse amplitude change must be less than

$$\frac{\Delta A}{A} = \frac{1}{316} = 0.00316 = 0.3 \text{ percent}$$

The A/D sampling time jitter must be less than

$$J = \frac{\tau}{316\sqrt{1}} = \frac{2 \times 10^{-6}}{316} = 6 \times 10^{-9} \text{ s}$$

Of the above requirements, the only ones that may be difficult to meet are the stalo stability[33,34] and the coho-locking accuracy. However, in systems with large bandwidths (short compressed pulses) the timing jitter requirements become significant and may require special clock regeneration circuitry at key system locations.

Effect of Quantization Noise on Improvement Factor. Quantization noise, introduced in the A/D converter, limits the attainable MTI improvement factor. Consider a conventional video MTI system, as shown in Fig. 15.49. Because

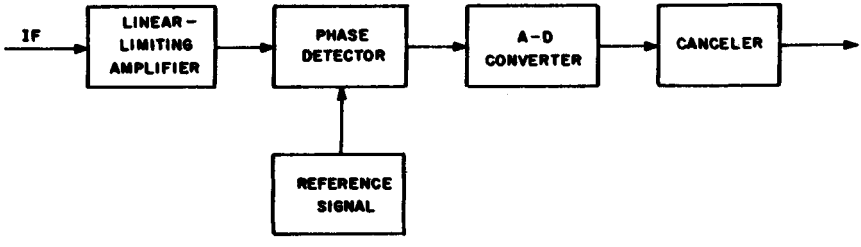

FIG. 15.49 Digital MTI consideration.

the peak signal level is controlled by the linear-limiting amplifier, the peak excursion of the phase-detector output is known, and the A/D converter is designed to cover this excursion. If the A/D converter uses N bits and the phase-detector output is from -1 to $+1$, the quantization interval is $2/(2^N - 1)$. The rms value of the signal-level deviation introduced by the A/D converter is $2/[(2^N - 1)\sqrt{12}]$. The limit on the MTI improvement factor that this imposes on a signal reaching the full excursion of the phase detector is found by substituting in the following equation from Table 15.4.

$$I = 20 \log \frac{A}{\Delta A} = 20 \log \left\{ \frac{1}{[(2^N - 1)\sqrt{3.0}]^{-1}} \right\} = 20 \log [(2^N - 1)\sqrt{3.0}] \tag{15.34}$$

Because two quadrature channels contribute independent A/D noise, the average limit on the improvement factor of a full range signal is

$$I = 20 \log \left[(2^N - 1) \sqrt{\frac{3.0}{2}} \right] = 20 \log [(2^N - 1)\sqrt{1.5}] \tag{15.35}$$

If the signal does not reach the full excursion of the A/D converter, which is normally the case, then the quantization limit on I is proportionately more severe. For example, if the system is designed so that the mean level of the strongest clutter of interest is 3 dB below the A/D converter peak, the limit on I would be $20 \log [(2^N - 1)\, 0.75]$. (This is tabulated in Table 15.5.)

TABLE 15.5 Typical Limitation on I Due to A/D Quantization

Number of bits, N	Limit on MTI improvement factor I, dB
4	22.3
5	28.6
6	34.7
7	40.8
8	46.9
9	52.9
10	59.0
11	65.0
12	71.0

This discussion of A/D quantization noise has assumed perfect A/D converters. Many A/D converters, particularly under high-slew-rate conditions, are less than perfect. This in turn leads to system limitations more severe than predicted here. (See Sec. 15.12.)

Substituting the pulse-to-pulse rms deviation for ΔA in Eq. (15.34) was done on the assumption that the pulse-to-pulse quantization error is independent. Brennan and Reed[35] have calculated a *quieting effect* which occurs when the quantization interval is coarse compared with the clutter change between pulses (which results in a number of successive pulses out of the A/D converter having

the same level), but this quieting effect will not occur with practical system parameters.

Pulse Compression Considerations. When an MTI system is used with pulse compression, the system target detection capability in clutter may be as good as a system transmitting the equivalent short pulse, or the performance may be no better than a system transmitting the same-length uncoded pulse. The kind of clutter environment, the system instabilities, and the signal processing utilized determine where the system performance will fall between the above two extremes. Unless provision is incorporated for coping with system instabilities, the MTI pulse compression system may fail to work at all in a clutter environment.

Ideally, a pulse compression receiver coupled with an MTI would appear as in Fig. 15.50*a*. If the pulse compression system were perfect, the compressed pulse would look as if the radar had transmitted and received a short pulse, and MTI processing could proceed as if the pulse compression had not existed. In practice,

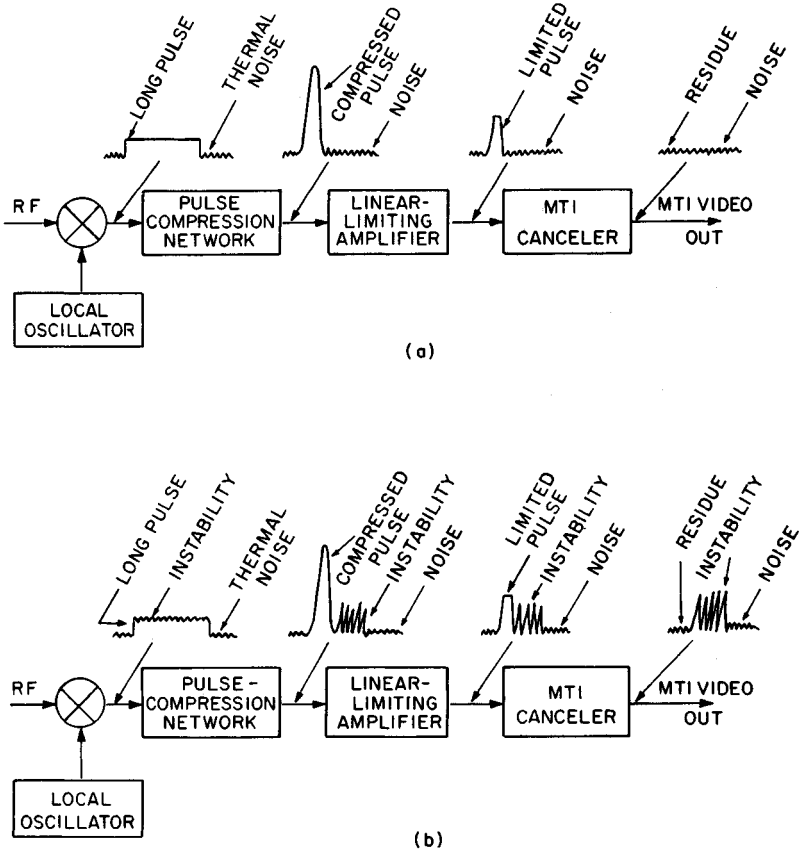

FIG. 15.50 Pulse compression with MTI. (*a*) Ideal but difficult-to-achieve combination. (*b*) Effect of oscillator on transmitter instabilities.

the compressed pulse will have time sidelobes from two basic causes. The first is system design, components that may be nonlinear with frequency, etc. These sidelobes will be stable; that is, they should repeat precisely on a pulse-to-pulse basis. The second cause of pulse compression sidelobes is system instabilities, such as noise on local oscillators, noise on transmitter power supplies, transmitter time jitter, and transmitter tube noise. These sidelobes are noiselike and are proportional to the clutter amplitude. For example, assume that the noiselike component of the sidelobes is down 40 dB from the peak transmitted signals. This noiselike component will not cancel in the MTI system, and therefore, for each clutter area that exceeds the system threshold by 40 dB or more, the residue will exceed the detection threshold. If the clutter exceeds the threshold by 60 dB, the residue from the MTI system will exceed the detection threshold by 20 dB, eliminating the effectiveness of the MTI. Figure 15.50*b* is a sketch of this effect.

One approach that has been successful in achieving the maximum MTI system performance attainable within the limits imposed by system and clutter instabilities is shown in Fig. 15.51. (Transmitter noise will be used in the following discussion to represent all possible system instabilities that create noiselike pulse compression time sidelobes.)

Limiter 1 is set so that the dynamic range at its output is equal to the range between peak transmitter power and transmitter noise in the system bandwidth. Limiter 2 is set so that the dynamic range at its output is equal to the expected MTI improvement factor. These limiter settings cause the residue due to transmitter noise and the residue due to other instabilities, such as quantization noise and internal-clutter motion, each to be equal to front-end thermal noise at the canceler output. This allows maximum sensitivity without an excessive false-alarm rate. The limiters are adjustable so that, when the system is placed in the field, they can be adjusted to take advantage of all the equipment and clutter stability that exists while precisely controlling the number of false alarms at the threshold output. Limiter 1 is a very efficient constant-false-alarm-rate device against transmitter noise because it suppresses the noise in direct proportion to the clutter signal strength but does not suppress at any time when the clutter signal is not strong. Thus a weak target that overlaps a strong piece of clutter by half of the uncompressed pulse length will be 50 percent suppressed, but the remaining 50 percent will be recompressed in the pulse compression network (with 6 dB amplitude loss) and can still be detected.

Although the limiter causes partial or complete suppression of some desired targets in the clutter areas, no targets are suppressed that could otherwise have been detected in the presence of transmitter noise at the system output if the limiter had not been used.

As a specific example, consider a system with a pulse compression ratio of about 30 dB and transmitter noise in the 15-MHz system noise bandwidth approximately 28 dB below the carrier power. (This is considered typical.[36]) Assume that the MTI canceler improvement factor is 30 dB, limited by clutter motion (internal-clutter spectral spread). With the above system parameters, a receiver

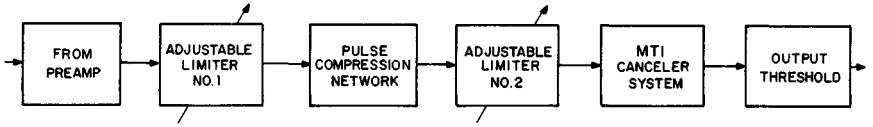

FIG. 15.51 Practical MTI pulse compression combination.

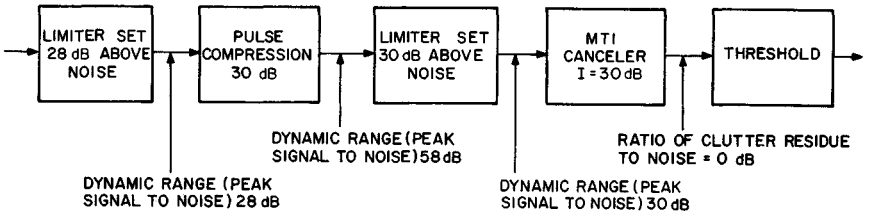

FIG. 15.52 MTI with pulse compression.

system that will provide the maximum obtainable performance should be adjusted as shown in Fig. 15.52. At the output of the pulse compression network, the transmitter noise will be equal to or less than thermal noise for either distributed clutter or point clutter. The peak clutter signals will vary from 28 dB above thermal noise for evenly distributed clutter to 58 dB above thermal noise for strong point clutter.

Because the MTI canceler is expected to attenuate clutter by 30 dB, the second limiter is provided to prevent the residue from strong clutter from exceeding the threshold. Without the second limiter, a strong-point reflector that was 58 dB above noise at the canceler input would have a residue 28 dB above noise at the canceler output. This would be indistinguishable from an aircraft target.

If the transmitter noise were 15 dB less than assumed above, the first limiter would be set 43 dB above thermal noise and much less target suppression would occur. Thus target detectability would improve in and near the strong clutter areas even though the MTI improvement factor was still limited to 30 dB by internal-clutter motion.

In summary, the noiselike pulse compression sidelobes and the duration of the uncompressed pulse dictate how effective a pulse compression MTI system can be. Systems have been built in which transmitter noise and long uncompressed pulses combined to make the systems incapable of detecting aircraft targets in or near land clutter. On the other hand, systems with low transmitter noise or with a short uncompressed pulse have proved satisfactory. Some existing pulse compression systems have not deliberately provided the two separate limiters described above, but the systems work because dynamic range is sufficiently restricted by circuit components. Other systems, such as those that deliberately hard-limit before pulse compression for CFAR reasons, do not have clutter residue problems but suffer from significant target suppression in the clutter areas.

An alternative to the use of limiters is the use of clutter maps. For the clutter maps to be successful in preventing detections from transmitter noise reflected from clutter and then dispersed in the pulse compression process, the clutter maps must be applied to the MTI filter outputs. Thus the clutter residue builds up in the maps, preventing detections on the residue in the filter outputs.

15.12 ANALOG-TO-DIGITAL CONVERSION CONSIDERATIONS

The accurate conversion of the radar IF signal into an equivalent digital representation is an important step in the implementation of a modern digital signal processor. This A/D conversion must preserve the amplitude and phase informa-

tion contained in the radar returns with a minimum of error if the subsequent digital MTI or MTD processing is to provide the predicted level of performance. Figure 15.53 shows the block diagram of a typical I and Q phase detector circuit and the associated A/D converters and indicates the various error sources as discussed in detail below. Since most A/D converters will not provide predictable output codes when the input voltage exceeds their full-scale range, an amplitude limiter must be included at IF to ensure that it is impossible to drive the A/D converter beyond its maximum input value. More important, if limiting is allowed to occur at the A/D converter, severe harmonics will be introduced in the digital signal representation and the performance of a doppler filter bank will become unpredictable and most probably very poor. The two coherent phase detectors (balanced mixers) are driven by in-phase and quadrature CW signals from the coho. Harmonic outputs are removed by the low-pass filters. The resulting in-phase and quadrature representation of the amplitude and phase of the IF signal are then converted to an equivalent digital representation by the A/D converters, which are assumed to include the necessary sample-and-hold circuits. The error sources indicated in the diagram are as follows: (*a*) A phase detector nonlinearity which is caused by gain compression in the balanced mixer. This occurs if the power of the coho reference signal is not sufficiently higher than the largest input signal. (*b*) A quadrature phase error in the applied coho reference signals which distorts the reference coordinate system of the I and Q representation of the signal. (*c*) A gain error in one of the I or Q channels. This also distorts the reference coordinate system. (*d*) A dc offset at the input to the A/D converter. This is equivalent to a zero-doppler CW signal component. (*e*) The amplitude quantization due to the finite number of bits in the A/D converter. The effect of this quantization on the maximum improvement factor was discussed in Sec. 15.11.

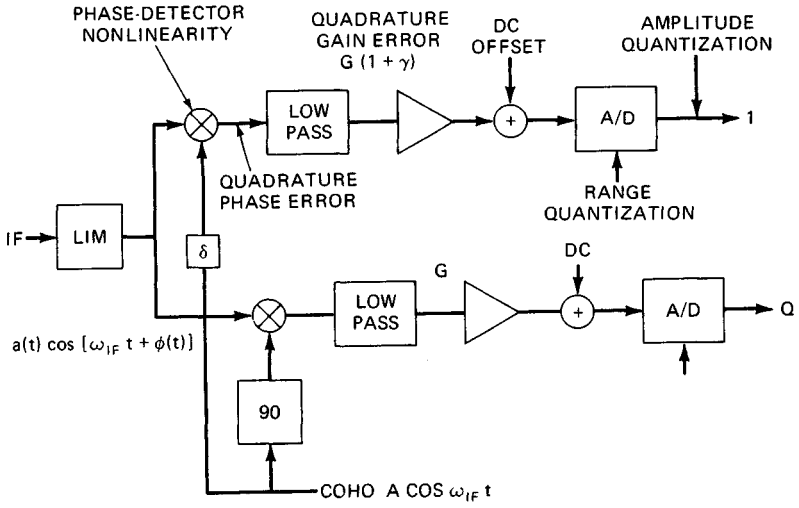

FIG. 15.53 Error sources in radar quadrature detection and A/D conversion.

Dynamic Range. The dynamic range of an A/D converter is limited by the number of bits in the output word. The quantization noise of an A/D converter has an rms value which is $N_Q = 1\sqrt{12}$ relative to the least significant bit (LSB). For an L-bit A/D converter the maximum amplitude which can be converted is proportional to 2^{L-1} (the most significant bit represents the sign), so that the maximum dynamic range is

$$DR_{max} = 2^{(L-1)}\sqrt{12} \tag{15.36}$$

As an example, a 10-bit A/D converter will have a maximum dynamic range of 65.0 dB.

In a practical system the maximum dynamic range must be reduced because thermal noise at the input to the A/D must be well above the quantization noise in order to preserve the system noise figure and because the rms value of a sinusoidal signal is a factor of $\sqrt{2}$ below the peak value. The latter factor reduces the practical dynamic range by 3 dB. The rms noise level of system noise at the A/D input is usually set so that the rms value of the noise into the A/D converter is equal to the voltage increment corresponding to one to two levels. The number of levels corresponding to the rms noise level will be denoted k. Thus, the available dynamic range (voltage ratio) is

$$DR_{actual} = \frac{2^{(L-1)}}{\sqrt{2}}\frac{1}{k} \tag{15.37}$$

since $2^{L-1}\sqrt{2}$ is the rms value of the maximum signal and k is the rms value of the noise. Thus for a 10-bit A/D converter and a noise level set at $k = 2.0$ the actual dynamic range would be 45.2 dB, almost 20 dB below the theoretical maximum.

From the value of the quantization noise ($N_Q = 1/12$) and the actual thermal noise at the output of the A/D converter, the noise figure degradation due to the quantization noise is found as

$$L_Q = 10 \log\left(\frac{k^2 + N_Q}{k^2}\right) \quad \text{dB} \tag{15.38}$$

which for $k = 2.0$ is $L_Q = 0.09$ dB. For $k = 1.0$ the quantization loss is increased to $L_Q = 0.35$ dB, while the dynamic range is increased by 6 dB. The need to maintain an adequate level of noise in the signal processor to allow effective operation of CFAR processing circuits tends to favor a value of the input noise close to two levels ($k = 2.0$).

***I* and *Q* Balance Requirements.** During the transformation of the amplitude and phase information in the IF signal into an equivalent representation in rectangular coordinates, dc offsets, amplitude imbalance, and phase errors are introduced. DC offsets which represent a spectral line at zero doppler at the A/D converter output can be compensated for quite readily. By implementing a long time-constant averaging circuit at the A/D converter output the dc component can be estimated and subtracted in each of the I and Q channels.

The effect of amplitude imbalance and phase errors is to generate spurious sidebands at the image doppler frequency corresponding to signals and clutter at the input. For clutter at zero doppler this sideband will also be located at zero doppler, and therefore it will not affect MTI performance. For doppler-shifted clutter returns which are suppressed by an MTI filter with an offset notch, the level of this sideband becomes a limiting factor on the improvement factor because it may be located at a doppler frequency at which the MTI filter has little or no attenuation. A calculation of the relative level of the spurious sideband caused by amplitude and phase imbalance has been made by Sinsky and Wang.[37] A graph showing the sideband level as a function of the quadrature error in ampli-

tude or phase is shown in Fig. 15.54. In order to make this sideband less than −40 dB, the amplitude error must be less than 0.17 dB and the quadrature phase error less than 1.1°.

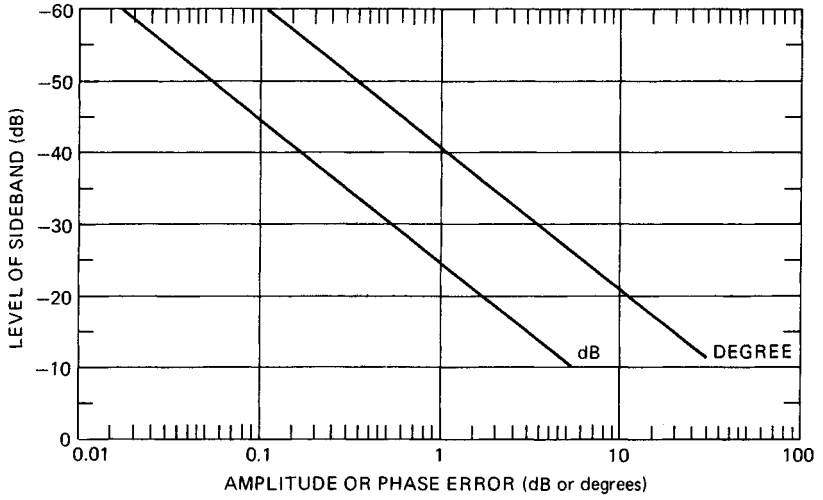

FIG. 15.54 Image sideband due to I and Q amplitude and phase errors.

Timing Jitter. The effect of timing jitter in the clock controlling the sample-and-hold circuit at the input to the A/D converter is equivalent to timing jitter on the transmitted pulse as discussed in Sec. 15.11. Its effect must therefore be included in the overall system stability budget for allowable timing jitter.

Linearity. For A/D converters with a large number of bits, the design of the coherent detectors needed to obtain the I and Q information becomes a compromise between noise figure and linearity. Any compression of the dynamic range at the limit of the input range will result in the generation of spurious outputs. If the nonlinearity is odd, symmetric odd harmonics will be generated. Calculations have shown that this sideband will be at about −48 dB when the dynamic-range compression is 0.1 dB at the maximum signal amplitude and about −31 dB when the dynamic-range compression reaches 1 dB. This effect is again important only when clutter at nonzero doppler has to be canceled in a filter with an offset rejection notch.

Accuracy. A/D converters are not necessarily perfect, as the discussion above has assumed. It is recommended that an A/D be evaluated with large signals at all frequencies within the receiver passband to establish that the quantization noise is as low as theoretically expected and that no spurious signals are produced. A/Ds with noise larger than theoretical are still usable, but it is necessary to consider their reduced performance in establishing system performance. For example, a

noisy 14-bit A/D might be evaluated as being equivalent to a perfect 12-bit A/D converter.

15.13 ADAPTIVE MTI IMPLEMENTATION

When the doppler frequency of the returns from clutter is unknown at the radar input, special techniques are required to guarantee satisfactory clutter suppression. As discussed in Sec. 15.8, the doppler filter bank will usually be effective against moving clutter. This requires that the individual filters be designed with a low sidelobe level in the regions where clutter may appear and that each filter be followed by appropriate CFAR processing circuits to reject unwanted clutter residue. When clutter suppression is to be implemented with a single MTI filter, it is necessary to use adaptive techniques to ensure that the clutter falls in the MTI rejection notch. An example of such an adaptive MTI is TACCAR,[38] originally developed for airborne radars. In many applications the adaptive MTI will further have to take into account the situation where multiple clutter sources with different radial velocities are present at the same range and bearing.

Usually the doppler shift of clutter returns is caused by the wind field, and early attempts of compensating in the MTI have varied the coho frequency sinusoidally as a function of azimuth based on the average wind speed and direction. This approach is unsatisfactory because the wind field rarely is homogeneous over a large geographical area and because the wind velocity usually is a function of altitude due to wind shear (important for rain clutter and chaff). Against a single clutter source an implementation is required which permits the MTI clutter notch to be shifted as a function of range. An example of such an adaptive MTI implementation is shown in Fig. 15.55. The phase-error circuit compares the clutter return from one sweep to the next. Through a closed loop, which includes a smoothing time constant, the error signal controls a phase shifter at the coho output such that the doppler shift from pulse to pulse is removed. It should be noted that since the first sweep entering the MTI is taken as a reference, any phase shift run-out as a function of range will increase proportionally to the number of sweeps. Ultimately this run-out will exceed the speed of

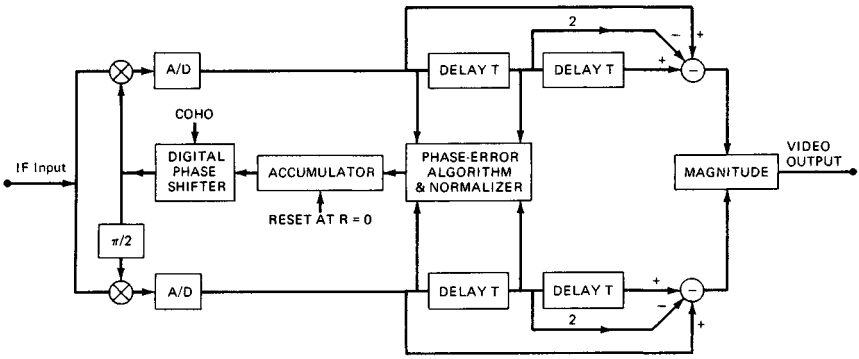

FIG. 15.55 Block diagram of closed-loop adaptive digital MTI.

response of the closed loop, and the MTI must be reset. This type of closed-loop adaptive MTI must therefore be operated for a finite set (batch) of pulses to ensure that this will not happen. Such batch-mode operation is also required if a combination of MTI operation and frequency agility is desired.

If a bimodal clutter situation is caused by the simultaneous presence of returns from land clutter and weather or chaff, an adaptive MTI can be implemented following a fixed-clutter-notch MTI section as illustrated in Fig. 15.56. The number of zeros used in the fixed- (zero-doppler) clutter-notch section of the MTI is determined by the required improvement factor and the spectral spread of the land clutter. Typically the fixed-notch MTI would use two or three zeros. For the adaptive portion of the MTI a fully digital implementation is shown in which the pulse-to-pulse phase shift of the clutter output from the first canceler is measured and averaged over a given number of range cells. This estimated phase shift is added to the phase shift which was applied to the data on the previous sweep, and this new phase shift is applied to the current data. The range averaging must be performed separately on the I and Q components of the measured phase in each range cell due to the 2π ambiguity of the phase representation itself. The accumulation of the applied phase shift from sweep to sweep, however, must be performed directly on the phase and is computed modulo 2π. The number of zeros of the adaptive MTI section is again determined by the required improvement factor and the expected spectral spread of the clutter. The phase shift is applied to the input data in the form of a complex multiply which again requires the transformation of the phase angle into rectangular coordinates. This transformation can easily be performed by a table lookup operation in a read-only memory.

When doppler shifts are introduced by digital means as described above, the accuracy of the I and Q representation of the original input data becomes an important consideration. Any dc offset, amplitude imbalance, quadrature phase error, or nonlinearity will result in the generation of undesired sidebands that will appear as residue at the canceler output. A discussion of A/D conversion considerations was presented in Sec. 15.12.

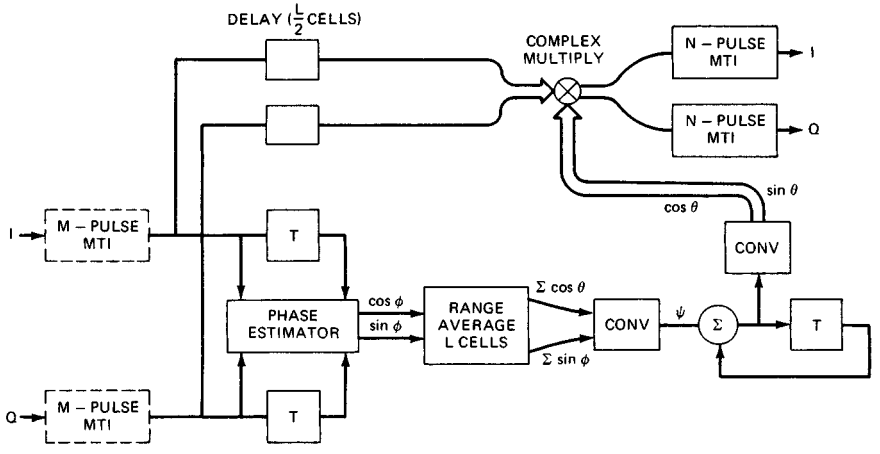

FIG. 15.56 Open-loop adaptive MTI for cancellation of simultaneous fixed and moving clutter.

In the adaptive MTI implementation described above the number of zeros allocated to each of the two cancelers was fixed, based on an a priori assessment of the clutter suppression requirement. The only variation possible would be to completely bypass one (or both) of the MTI cancelers if no land clutter or weather or chaff returns are received on a given radial. A more capable system can be implemented if the number of zeros can be allocated dynamically to either clutter source as a function of range. This leads to a fully adaptive MTI implementation using a more complex adaptation algorithm, as discussed below. Such an adaptive MTI may provide a performance close to the optimum discussed in Sec. 15.6.

In order to illustrate the difference in performance between such candidate MTI implementations, a specific example is considered next. For this example, land clutter returns are present at zero doppler with a normalized spectral spread of $\sigma_f T = 0.01$, and chaff returns are present at a normalized doppler offset of $f_d T = 0.25$ with a normalized spectral spread of $\sigma_f T = 0.05$. The power ratio of the land clutter to that of the chaff is denoted Q (dB). Thermal noise is not considered in this example. In both cases the total number of filter zeros was assumed to be equal to three. For the adaptive MTI with a fixed allocation of zeros, two zeros are located at zero doppler and the remaining zero is centered on the chaff returns. In the optimum MTI the zero locations are chosen so that the overall improvement factor is maximized. The results of this comparison are presented in Fig. 15.57, which shows the improvement factor for the optimum and the adaptive MTI as a function of the power ratio Q (dB). When Q is small so that chaff returns dominate, a significant performance improvement can be realized by using all MTI filter zeros to cancel the chaff returns. The performance difference for large values of Q is a result of an assumption made that the location of the third zero remains fixed at the chaff doppler frequency. In reality, the adaptive MTI would move its third zero to the land clutter as the land clutter residue starts to dominate the output of the first canceler. The zero locations of the optimum MTI are shown in Fig. 15.58 and can be seen to move between the land clutter at zero doppler toward the doppler of the chaff returns as the relative level of the land clutter becomes small.

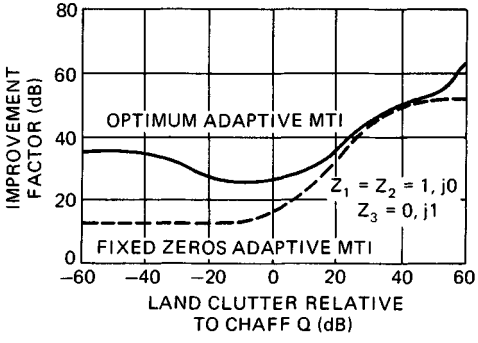

FIG. 15.57 Improvement factor comparison of optimum and adaptive MTI against fixed and moving clutter of ratio Q.

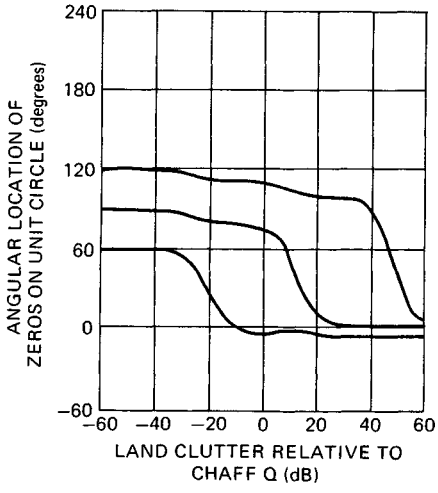

FIG. 15.58 Location of filter zeros for optimum MTI used against fixed and moving clutter.

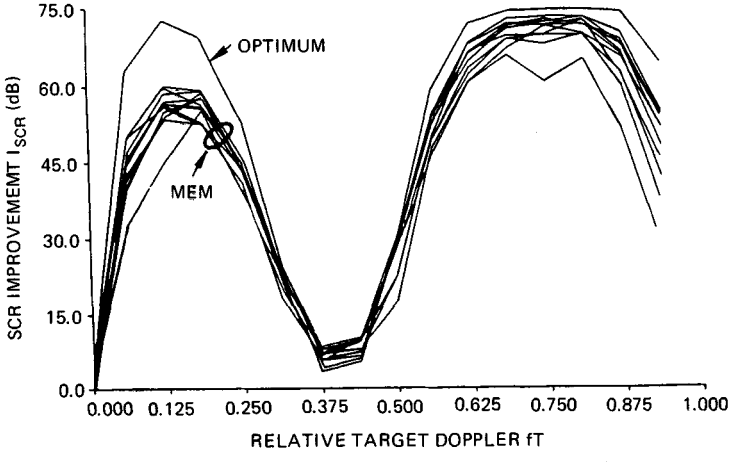

FIG. 15.59 Performance of an adaptive MTI based on the maximum-entropy spectral estimation theory.

The implementation of a fully adaptive MTI can be based on modern techniques of spectral estimation, as represented by the maximum-entropy method (MEM).[39] An example of the performance obtained through the use of an MTI based on the MEM principle is shown in Fig. 15.59. For this example bimodal clutter returns were assumed, consisting of land clutter at zero doppler 60 dB above noise having a relative spectral spread of $\sigma_f T = 0.01$ and 60 dB chaff returns at a normalized doppler frequency of $f_d T = 0.4$ with a relative spectral spread of $\sigma_f T = 0.06$. The total number of pulses processed in one coherent processing interval is CPI = 16. The MEM algorithm was implemented by using a lattice filter estimating seven poles of the clutter spectrum based on the 16 re-

turns and by subsequently processing the 16 returns through a matching seven-zero FIR filter. The results of 12 independent simulation runs are shown in Fig. 15.59, and the optimum filter response is shown for reference.

15.14 CLUTTER MAP IMPLEMENTATION

In many MTI radar applications the clutter-to-noise ratio in the receiver will exceed the improvement factor limit of the system even when techniques such as sensitivity time control (STC), improved radar resolution, and reduced antenna gain close to the horizon are used to reduce the level of clutter returns. The resulting clutter residues after the MTI canceler must therefore be further suppressed to prevent saturation of the PPI display and/or an excessive false-alarm rate in an automatic target detection (ATD) system.

Against spatially homogeneous sources of clutter such as rain, sea clutter, or corridor chaff, a cell-averaging constant-false-alarm-rate (CFAR) processor following the MTI filter will usually provide good suppression of the clutter residues. Special features are sometimes added to the CFAR, such as greatest-of selection or two-parameter (scale and shape) normalization logic, in order to improve its effectiveness at clutter boundaries or if the probability distribution of the clutter amplitude is nongaussian. However, when the clutter returns are significantly nonhomogeneous, as is the case for typical land clutter returns, the performance of the cell-averaging CFAR will not be satisfactory and other means must be implemented to suppress the output clutter residues to the noise level.

The traditional solution to this problem has been to deliberately reduce the receiver dynamic range prior to the MTI filter to the same value as the maximum system improvement factor. Theoretically, then, the output residue should be at or below the normal receiver noise level, and no false alarms would be generated. In practice, the introduction of IF limiting against the ground clutter returns will result in an additional improvement factor restriction, as discussed in Sec. 15.10. Consequently, for the limited IF dynamic range to have the desired effect on the output residues, the limit level must be set 5 to 15 dB below the improvement factor limit of the linear system. The net result is that some of the clutter suppression capability of the MTI radar must be sacrificed in exchange for control of the output false-alarm rate.

Since returns from land clutter scatterers usually are spatially fixed and therefore appear at the same range and bearing from scan to scan, it has long been recognized that a suitable memory circuit could be used to store the clutter residues and remove them from the output residue on subsequent scans by either subtraction or gain normalization. This was the basic principle of the so-called area MTI, and many attempts have been made to implement an effective version of this circuit over an extended span of time. The main hindrance to its success has been the lack of appropriate memory technology, since the storage tube (long the only viable candidate) lacks in resolution, registration accuracy, simultaneous read-and-write capability, and stability. The development of high-capacity semiconductor memories is the technological breakthrough that has made the design of a working area MTI a reality. The *area MTI* is better known today as a *clutter map*, but both terms are used.

The clutter map may be considered as a type of CFAR where the reference samples, which are needed to estimate the level of the clutter (or clutter residue), are collected in the cell under test on a number of previous scans. Since aircraft targets usually move several resolution cells from one scan to the next, it is un-

likely that the reference samples will be contaminated by a target return. Alternatively, by making the averaging time (in terms of past scans) long, the effect of an occasional target return can be minimized. While the primary purpose of the clutter map is to prevent false alarms due to discrete clutter or clutter residues which are at a fixed location, it may also be necessary to consider slowly moving point clutter in the clutter map design, either to suppress bird returns or because the radar is on a moving platform (e.g., a ship).

The memory of a clutter map is usually organized in a uniform grid of range and azimuth cells as illustrated in Fig. 15.60. Each map cell will typically have 8 to 16 bits of memory so that it will handle the full dynamic range of signals at its input and provide superclutter visibility when a target is flying over a point of clutter. The dimensions of each cell are a compromise between the required memory and several performance characteristics. These are the cutoff velocity of the map, its transient response, and the loss in sensitivity caused by the clutter map (similar to a CFAR loss). The minimum cell size will be constrained by the size of the radar resolution cell.

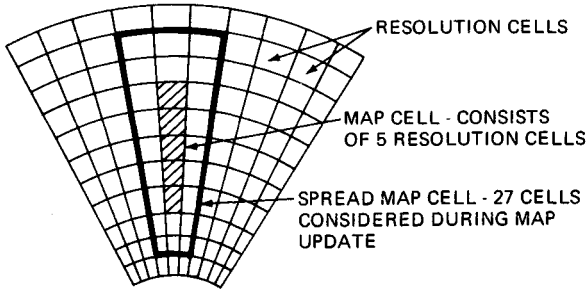

FIG. 15.60 Clutter map cell definition.

Each map cell is updated by the radar returns (or residues) falling within its borders (or in its vicinity) on several previous scans. To save memory the cells are usually updated by using a simple recursive (single-pole) filter of the form

$$y(i) = (1 - \alpha) \times y(i - 1) + \alpha x(i) \tag{15.39}$$

where $y(i - 1)$ is the old clutter map amplitude, $y(i)$ is the updated clutter map amplitude, $x(i)$ is the radar output on the present scan, and the constant α determines the memory of the recursive filter. The test for detecting a target based on the output $x(i)$ is

$$x(i) \geq k_T y(i - 1) \tag{15.40}$$

where the threshold constant k_T is selected to give the required false-alarm rate. Alternatively, the radar output can be normalized on the basis of the clutter map content to obtain an output $z(i) = x(i)/y(i - 1)$, which can be processed further if required. Analogously to the implementation of the cell-averaging CFAR processor, the amplitude $x(i)$ can be in linear, square-law, or logarithmic units.

The loss in detectability due to the clutter map is analogous to the CFAR loss analyzed in the literature for many different conditions. An analysis of the clutter map loss for single-hit detection using a square-law detector has been presented by Nitzberg.[40] These and other results can be summarized into a single universal

curve of clutter map loss, L_{CM}, as a function of the ratio x/L_{eff}, as shown in Fig. 15.61, where x defines the required false-alarm probability according to $P_f = 10^{-x}$ and L_{eff} is the effective number of past observations averaged in the clutter map defined as

$$L_{eff} = \frac{2 - \alpha}{\alpha} \tag{15.41}$$

For example, for $P_f = 10^{-5}$ and $\alpha = 0.125$ the clutter map loss is $L_{CM} = 1.8$ dB since $x = 5$ and $L_{eff} = 15$ for this case. Also shown in Fig. 15.61 is the curve for the conventional cell-averaging CFAR,[41] where all reference samples are equally weighted. If more than one noise amplitude is used to update the clutter map content on each scan, the value of L_{eff} should be increased proportionally.

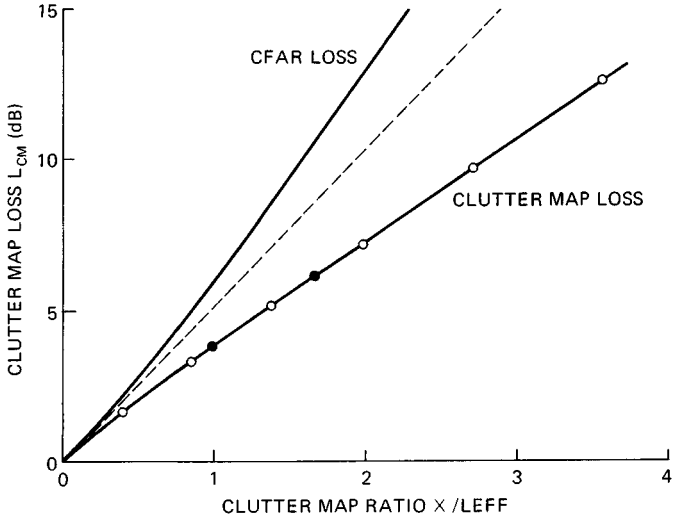

FIG. 15.61 Universal curve for determining detectability loss caused by the clutter map.

An analysis of the performance of typical implementations of clutter maps has been presented by Khoury and Hoyle.[42] From this reference a typical transient-response curve is shown in Fig. 15.62 for a Rayleigh fading point clutter source 20 dB above thermal noise, a filtering constant of $\alpha = 0.125$, and assuming four returns noncoherently integrated in each clutter map cell. The abscissa is in radar scans, and the ordinate is probability of detection of the point clutter source. Since the clutter point has the same amplitude statistics as thermal noise, the output false-alarm rate approaches $P_f = 10^{-6}$ asymptotically.

Against a slowly moving source of clutter (e.g., birds) the probability of detection may increase as the clutter source crosses the boundary between two clutter map cells. To prevent this a spreading technique can be used which will update each clutter map cell, not only with radar returns falling within its boundaries but also by using radar returns in adjacent cells in range and azimuth. Through the use of such spreading an additional degree of control over the clutter map velocity response can be achieved. An example of

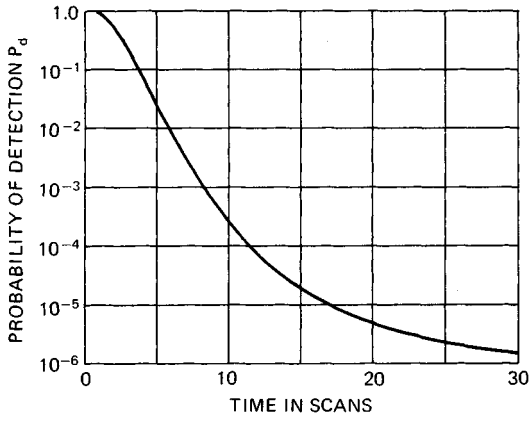

FIG. 15.62 Transient response of clutter map due to Swerling Case 2 point clutter model. (*From Khoury and Hoyle.*)[42]

the velocity response of a clutter map including such spreading is shown in Fig. 15.63. The range extent of the clutter map cell is 5 μs, the radar resolution cell is 1 μs, $n = 4$ pulses are noncoherently integrated, the filtering constant is $\alpha = 0.125$, the scan time is 5 s (12 r/min), and the $SNR = 20$ dB. On each scan, the clutter map cell is updated with the radar amplitudes in the five range cells falling within the clutter map cell and with the amplitude from one additional radar resolution cell before and after the clutter map cell. It is seen from Fig. 15.63 that the velocity response characteristic of the clutter map from stopband to passband is somewhat gradual in this particular implementation. This is partly due to the large size of the clutter map cell relative to the radar resolution. A finer-grain map with additional spreading would have a much better velocity response characteristic.

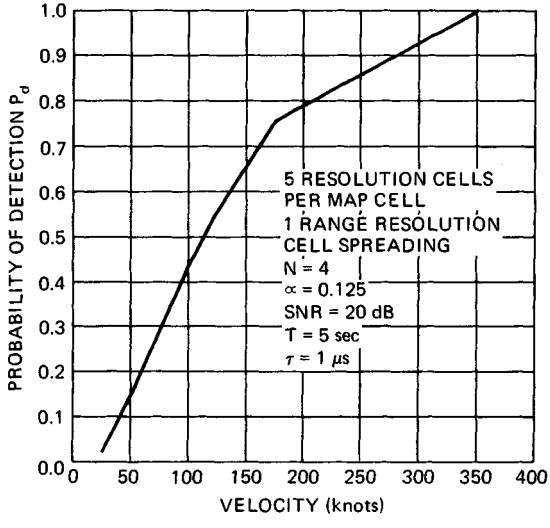

FIG. 15.63 Velocity response of clutter map.

A potential problem with the type of amplitude clutter map described in this section is the fact that a large target flying in front of a smaller target may cause enough buildup in the map to supress the small target. One way to overcome this problem in a system which includes automatic tracking would be to use the track prediction gate to inhibit updating of the clutter map with new (target) amplitudes.

15.15 CONSIDERATIONS APPLICABLE TO MTI RADAR SYSTEMS

MTI radar system design encompasses much more than receiver design. The entire radar system—transmitter, antenna, and operational parameters—must be keyed to function as part of an MTI radar. For example, excellent MTI circuitry will not perform satisfactorily unless the radar local oscillator is extremely stable, the transmitter has almost no pulse-to-pulse frequency or phase jitter, and the time on target is sufficient for coherent rejection of unwanted signals.

The design of MTI radar systems requires a number of compromises. One of the most serious problems is that desired targets often have radial velocities that are less than those of undesired targets. When a target flies past a radar, there is an interval when the doppler frequency passes through zero and the target is cancelled. This interval can be minimized by shaping the velocity response, but only at the expense of reducing the attainable improvement factor and increasing the response to undesired moving targets.

There are two classes of undesired moving targets that are particularly troublesome. These are typified by birds and automobiles. A large bird, such as a gull, crow, or buzzard, has a radar cross section of about 0.01 m^2 and flies 20 to 30 mi/h in still air. These flying speeds, combined with 10 to 20 mi/h winds, cause the birds often to fly at or near the velocity of the maximum MTI response. If there is one bird per square mile in the vicinity of the radar, there are over 1000 birds within 20 mi, which may saturate an automatic detection system and make a PPI display virtually useless. One approach to solving the bird problem that has been implemented on the air route surveillance radars[43–45] of the Federal Aviation Administration (FAA) is described below.

STC (sensitivity time control) can be employed to distinguish between small (0.01-m^2) targets and desired aircraft (1-m^2) targets. If the STC is programmed with a fourth-power law as a function of range, most of the bird returns can be eliminated from the display but desired targets are retained. The use of STC with a cosecant-squared antenna beam solves one problem but creates another: it also eliminates desired targets at high elevation angles where the antenna gain is low. The solution to this problem is to boost the antenna gain at high elevation angles to be considerably higher than the requirement for the cosecant-squared pattern. Not only does this compensate for the use of STC, but it also considerably enhances the target-to-clutter signal ratio for targets at high elevation angles, thus improving MTI performance. The penalty for this solution is a loss in the peak antenna gain which be achieved. An illustration of this approach is provided in Fig. 15.64, which shows the ARSR-2 antenna pattern and the corresponding free-space coverage. The loss in peak gain for this example, due to the boost of coverage at high angles, was about 2 dB.

The automobile and truck problem is more difficult to solve. The radar cross section of an automobile is as large as that from desired targets, and automobile speeds are well up in the response curves of most surveillance radars. If the radar is sited so that it can see many miles of highways, which is frequently the case in populated areas, automobiles are a major problem.

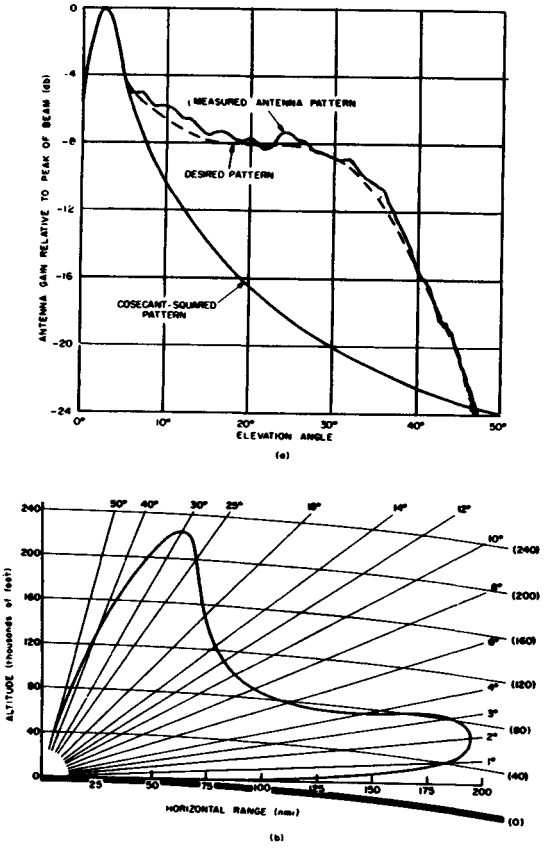

FIG. 15.64 Antenna elevation pattern for the ARSR-2 antenna. (*a*) Compared with the cosecant-squared pattern. (*b*) Free-space-coverage diagram.

One approach to solving the automobile problem is described in Refs. 46 and 47. On a horn-fed reflector antenna, a second horn is mounted beneath the primary horn to provide a high-angle receive-only beam. The energy is transmitted through the primary horn. The second horn is used for receiving for the first 20 mi, after which the receiver is electronically switched to the primary horn for the remainder of the interpulse interval. The use of the second beam at high angles greatly enhances the target-to-clutter signal ratio as well as the target-to-automobile signal ratio. This technique also greatly alleviates the bird problem because birds generally appear at low elevation angles.

REFERENCES

1. Barlow, Edward J.: Doppler Radar, *Proc. IRE*, vol. 37, pp. 340–355, April 1949.
2. Barton, David K.: "Radar System Analysis," Prentice-Hall, Englewood Cliffs, N.J., 1964.

3. Goldstein, Herbert: Sea Echo, the Origins of Echo Fluctuations, and the Fluctuations of Clutter Echoes, in Kerr, D. E. (ed.): "Propagation of Short Radio Waves," MIT Radiation Laboratory Series, vol. 13, McGraw-Hill Book Company, New York, 1951, secs. 6.6–6.21, pp. 560–587.
4. Wiltse, J. C., S. P. Schlesinger, and C. M. Johnson: Backscattering Characteristics of the Sea in the Region from 10 to 50 KMC, *Proc. IRE*, vol. 45, pp. 220–228, February 1957.
5. Hicks, B. L., N. Knable, J. J. Kovaly, G. S. Newell, J. P. Ruina, and C. W. Sherwin: The Spectrum of X-Band Radiation Back-Scattered from the Sea Surface, *J. Geophys. Res.*, vol. 65, pp. 828–837, March 1960.
6. Simkins, W. L., V. C. Vannicola, and J. P. Royan: Seek Igloo Radar Clutter Study, *Rome Air Development Center, Rept. TR*-77-338, October 1977. (DDC AD-A047 897.)
7. Nathanson, F. E., and J. P. Reilly: Radar Precipitation Echoes, *IEEE Trans.*, vol. AES-4, pp. 505–514, July 1968.
8. Barton, David K.: Radar Equations for Jamming and Clutter, *EASCON '67 Tech. Conv. Rec.*, Supplement to *IEEE Trans.*, vol. AES-3, pp. 340–355, November 1967.
9. Doviak, R. J., and D. S. Zrnić: "Doppler Radar and Weather Observations," Academic Press, Orlando, Fla., 1984.
10. "IEEE Standard Dictionary of Electrical and Electronics Terms," 3d ed., Institute of Electrical and Electronics Engineers, Inc., New York, 1984.
11. Barton, D. K., and W. W. Shrader: Interclutter Visibility in MTI Systems, *IEEE EASCON '69 Tech. Conv. Rec.*, pp. 294–297, October 1969.
12. Spafford, L.: Optimum Radar Signal Processing in Clutter, *IEEE Trans.*, vol. IT-14, pp. 734–743, September 1968.
13. Capon, J.: Optimum Weighting Functions for the Detection of Sampled Signals in Noise, *IEEE Trans.*, vol. IT-10, pp. 152–159, April 1964. (Reprinted in Ref. 14.)
14. Schleher, D. Curtis (ed.): "MTI Radar," Artech House, Norwood, Mass., 1978.
15. Skolnik, Merrill I.: "Introduction to Radar Systems," 2d ed., McGraw-Hill Book Company, New York, 1980.
16. White, W. D., and A. E. Ruvin: Recent Advances in the Synthesis of Comb Filters, *IRE Nat. Conv. Rec.*, vol. 5, pt. 2, pp. 186–200, 1957. (Reprinted in Ref. 14.)
17. Urkowitz, Harry: Analysis and Synthesis of Delay Line Periodic Filters, *IRE Trans.*, vol. CT-4, pp. 41–53, June 1957. (Reprinted in Ref. 14.)
18. Hall, W. M., and H. R. Ward: Signal-to-Noise Loss in Moving Target Indicator, *Proc. IEEE*, vol. 56, pp. 233–234, February 1968.
19. Shrader, W. W., and V. G. Hansen: Comments on "Coefficients for Feed-Forward MTI Radar Filters," *Proc. IEEE*, vol. 59, pp. 101–102, January 1971.
20. Fletcher, R. H., and D. W. Burlage: Improved MTI Performance for Phased Array in Severe Clutter Environments, *IEEE Conf. Publ. 105*, pp. 280–285, 1973.
21. Oppenheim, A. V., and R. W. Schafer: "Digital Signal Processing," Prentice-Hall, Englewood Cliffs, N.J., 1975.
22. Zverev, A. I.: Digital MTI Radar Filters, *IEEE Trans.*, vol. AU-16, pp. 422–432, September 1968.
23. Ludloff, A., and M. Minker: Reliability of Velocity Measurement by MTD Radar, *IEEE Trans.*, vol. AES-21, pp. 522–528, July 1985.
24. Grasso, G.: Improvement Factor of a Nonlinear MTI in Point Clutter, *IEEE Trans.*, vol. AES-4, pp. 640–644, November 1968.
25. Ward, H. R., and W. W. Shrader: MTI Performance Degradation Caused by Limiting, *EASCON '68 Tech. Conv. Rec.*, supplement to *IEEE Trans.*, vol. AE-4, pp. 168–174, November 1968.
26. Grasso, G., and P. F. Guarguaglini: Clutter Residues of a Coherent MTI Radar Receiver, *IEEE Trans.*, vol. AES-5, pp. 195–204, March 1969. (Reprinted in Ref. 14.)

27. Weil, T. A.: Applying the Amplitron and Stabilitron to MTI Radar System, *IRE Nat. Conv. Rec.*, vol. 6, pt. 5, pp. 120–130, 1958.

28. Weil, T. A.: An Introduction to MTI System Design, *Electron. Prog.*, vol. 4, pp. 10–16, May–June 1960.

29. Leeson, D. B., and G. F. Johnson: Short-Term Stability for a Doppler Radar: Requirements, Measurements and Techniques, *Proc. IEEE*, vol. 54, pp. 329–330, February 1966.

30. Hewlett-Packard Product Note 11729B-1, March 1984.

31. Vigneri, R., G. G. Gulbenkian, and N. Diepeveen: A Graphical Method for the Determination of Equivalent Noise Bandwidth, *Microwave J.*, vol. 11, pp. 49–52, June 1968.

32. Steinberg, Bernard D.: chaps. 1–4 in Berkowitz, R. S. (ed.): "Modern Radar: Analysis, Evaluation and System Design," pt. VI, John Wiley & Sons, New York, 1966, chaps. 1–4.

33. Stephenson, J. G.: Designing Stable Triode Microwave Oscillators, *Electronics*, vol. 28, pp. 184–187, March 1955.

34. Malling, L. R.: Phase Stable Oscillators for Space Communications, Including the Relationship between the Phase Noise, the Spectrum, the Short-Term Stability, and the Q of the Oscillator, *Proc. IRE*, vol. 50, pp. 1656–1664, July 1962.

35. Brennan, L. E., and I. S. Reed: Quantization Noise in Digital Moving Target Indications Systems, *IEEE Trans.*, vol. AES-2, pp. 655–658, November 1966. (Reprinted in Ref. 14.)

36. Bursweig, J., F. Hurt, and L. H. O'Brien: Intraspectral Noise and Transfer Functions of Pulsed Final Power Amplifiers, presented at *IEEE Electron. Devices Meet.*, Washington, Oct. 29, 1964.

37. Sinsky, A. I., and C. P. Wang: Error Analysis of a Quadrature Coherent Detection Processor, *IEEE Trans.*, vol. AES-10, pp. 880–883, November 1974.

38. Shrader, W. W.: MTI Radar, in Skolnik, M. I. (ed.): "Radar Handbook," McGraw-Hill Book Company, New York, 1970.

39. D'Addio, E., A. Farina, and F. A. Studer: The Maximum Entropy Method and Its Applications to Clutter Cancellation, *Riv. Tec. Selenia*, vol. 8, no. 3, pp. 15–24, 1983.

40. Nitzbert, R.: Clutter Map CFAR Anaysis, *IEEE Trans.*, vol. AES-22, pp. 419–421, July 1986.

41. Hansen, V. G.: Constant False Alarm Rate Processing in Search Radar, *IEE Conf. Publ.* 105, *Radar—Present and Future*, London, Oct. 23–25, 1973.

42. Khoury, E. N., and J. S. Hoyle: Clutter Maps: Design and Performance, *IEEE Nat. Radar Conf.*, Atlanta, 1984.

43. Shrader, W. W.: Antenna Considerations for Surveillance Radar Systems, *Proc. Seventh Ann. East Coast Conf. Aeronaut. Navig. Electron.*, October 1960.

44. Shrader, W. W.: Results of Antenna Pattern Considerations, *Proc. Eighth Ann. East Coast Conf. Aerosp. Navig. Electron.*, October 1961.

45. Shrader, W. W.: Reducing Clutter in Air Route Surveillance Radar, *Electronics*, pp. 37—41, Jan. 26, 1962.

46. Patrick, A. M.: Primary Radar in Air Traffic Control, *Interavia*, vol. 16, pp. 851—853, June 1961.

47. Mullholand, E. B., and F. R. Soden: Australia's ATC Radar Network, *Interavia*, vol. 22, pp. 511–513, Aprile 1967.